Evaluating the large-scale hydrological cycle response within the PlioMIP2 ensemble

Zixuan Han[1,2], Qiong Zhang[2], Qiang Li[2], Ran Feng[3], Alan M. Haywood[4], Julia C. Tindall[4], Stephen J. Hunter[4], Bette L. Otto-Bliesner[5], Esther C. Brady[5], Nan Rosenbloom[5], Zhongshi Zhang[6,7], Xiangyu Li[6], Chuncheng Guo[7], Kerim H. Nisancioglu[8,9], Christian Stepanek[10,11], Gerrit Lohmann[11], Linda E. Sohl[12,13], Mark A. Chandler[12,13], Ning Tan[14,15], Gilles Ramstein[15], Michiel L. J. Baatsen[16], Anna S. von der Heydt[16], Deepak Chandan[17], W. Richard Peltier[17], Charles J. R. Williams[18,19], Daniel J. Lunt[19], Jianbo Cheng[20], Qin Wen[21], Natalie J. Burls[22]

1. College of Oceanography, Hohai University, Nanjing, China
2. Department of Physical Geography and Bolin Centre for Climate Research, Stockholm University, Stockholm, Sweden
3. Department of Geosciences, College of Liberal Arts and Sciences, University of Connecticut, CT 06269, USA
4. School of Earth and Environment, University of Leeds, Woodhouse Lane, Leeds, West Yorkshire, UK
5. Climate and Global Dynamics Laboratory, National Center for Atmospheric Research, Boulder, CO 80305, USA
6. Department of Atmospheric Science, School of Environmental Studies, China University of Geosciences, Wuhan, China
7. NORCE Norwegian Research Centre, Bjerknes Centre for Climate Research, Bergen, Norway
8. Department of Earth Science, University of Bergen, Bjerknes Centre for Climate Research, Bergen, Norway
9. Centre for Earth Evolution and Dynamics, University of Oslo, Oslo, Norway
10. Institute for Environmental Physics, University of Bremen, Bremen, Germany
11. Alfred Wegener Institute-Helmholtz-Zentrum für Polar und Meeresforschung, Bremerhaven, Germany
12. Center for Climate Systems Research, Columbia University, New York, USA
13. NASA Goddard Institute for Space Studies, New York, USA
14. Key Laboratory of Cenozoic Geology and Environment, Institute of Geology and Geophysics, Chinese Academy of Sciences, Beijing, China
15. Laboratoire des Sciences du Climat et de l'Environnement, LSCE/IPSL, CEA-CNRS-UVSQ, Université Paris-Saclay, Gif-sur-Yvette, France
16. Institute for Marine and Atmospheric research Utrecht (IMAU), Department of Physics, Utrecht University, Utrecht, The Netherlands.
17. Department of Physics, University of Toronto, Toronto, Ontario, Canada
18. School of Geographical Sciences, University of Bristol, Bristol, UK
19. NCAS-Climate, Department of Meteorology, University of Reading, Reading, UK
20. School of Environmental Science and Engineering, Yancheng Institute of Technology, Yancheng, China
21. Key Laboratory for Virtual Geographic Environment, Ministry of Education; State Key Laboratory Cultivation Base of Geographical Environment Evolution of Jiangsu Province; Jiangsu Center for Collaborative Innovation in Geographical Information Resource Development and Application; School of Geography, Nanjing Normal University, Nanjing, China
22. Center for Ocean-Land-Atmosphere Studies, George Mason University, Fairfax, Virginia, USA

Correspondence to: Qiong Zhang (qiong.zhang@natgeo.su.se) and Zixuan Han (zixuan.han@hhu.edu.cn)

Abstract. The mid-Pliocene (~3 million years ago) is one of the most recent warm periods with high CO_2 concentrations in the atmosphere and resulting high temperatures and is often cited as an analog for near-term future climate change. Here, we apply a moisture budget analysis to investigate the response of the large-scale hydrological cycle at low latitudes within a

13-model ensemble from the Pliocene Model Intercomparison Project Phase 2 (PlioMIP2). The results show that increased atmospheric moisture content within the mid-Pliocene ensemble (the thermodynamic effect) results in wetter conditions over the deep tropics, i.e., the Pacific intertropical convergence zone (ITCZ) and the Maritime Continent, and drier conditions over the subtropics. The thermodynamic effect is to some extent offset by a dynamic effect involving a northward shift of the Hadley circulation that dries the deep tropics and moistens the subtropics in the Northern Hemisphere (i.e., the subtropical Pacific). From the perspective of Earth's energy budget, the enhanced southward cross-equatorial atmospheric transport (0.22 PW), induced by the hemispheric asymmetries of the atmospheric energy, favors an approximately 1° northward shift of the ITCZ. The shift of the ITCZ reorganizes atmospheric circulation, favoring a northward shift of the Hadley circulation. In addition, the Walker circulation consistently shifts westward within PlioMIP2 models, leading to wetter conditions over the northern Indian Ocean. The PlioMIP2 ensemble highlights that an imbalance of interhemispheric atmospheric energy during the mid-Pliocene could have led to changes in the dynamic effect, offsetting the thermodynamic effect and hence altering mid-Pliocene hydroclimate cycling.

1 Introduction

Earth's hydrological cycle can induce regional and global climate anomalies, thereby regulating the balance of global water resources (Eltahir and Bras, 1996). Many studies have indicated that pronounced climate change can occur as anthropogenic CO_2 rises, including an increase in surface temperature (Xie et al., 2010; Long et al., 2014), Arctic amplification (Stuecker et al., 2018; Smith et al., 2019), and impacts on animal and plant populations (Root et al., 2003). Under current global warming, both observations and model simulations suggest a tendency for the wet-regions-getting-wetter-and-dry-regions-getting-drier phenomenon (Held and Soden, 2006; Wentz et al., 2007; Chou et al., 2009; Wang et al., 2012; Li et al., 2013). That is, rainfall minus evaporation increases (decreases) in regions of climatological convergence (divergence). Note that these changes in the large-scale hydrological cycle could induce severe climatic disasters worldwide, leading to considerable impacts on economies, ecosystems, and agriculture (Asokan and Destouni, 2014; Bengtsson, 2014). Therefore, understanding the potential processes responsible for large-scale hydrological cycle changes in a warmer climate is of great importance.

Previous studies have suggested that the thermodynamic effect caused by increased atmospheric moisture content in a warmer climate is one of the primary contributors to a tendency of wet gets wetter and dry gets drier (Chou et al., 2009; Seager et al., 2010). This mechanism directly follows the nonlinearity of the Clausius-Clapeyron relationship, which acts to enhance the increase in atmospheric moisture content over regions with the warmest surface temperatures (Allen and Ingram, 2002; Stephens and Ellis, 2008). On the other hand, large-scale atmospheric circulation can change substantially due to nonuniform temperature changes under global warming and hence induce changes in the hydrological cycle via the so-called dynamic effect (Han et al., 2019a). The dynamic effect is relatively more complicated than the thermodynamic effect among climate models. Seager et al. (2010) demonstrated that the dynamic component is modulated by the weakening of the Hadley

circulation and Walker circulation. Increased CO_2 concentration could directly increase atmospheric static stability over tropical oceans, favoring a slowdown of these atmospheric overturning circulations (Vallis et al., 2015). Other studies have

75   indicated that local Hadley circulation shifts poleward due to the decreased meridional temperature gradient in response to increased CO_2 concentrations (Sharmila and Walsh, 2018; Hu et al., 2018a). These circulation anomalies widen the subtropical dry zones (Previdi and Liepert, 2007; Sun et al., 2013b). In addition, Long et al. (2016) highlighted that model uncertainty in tropical rainfall comes from the discrepancies of the atmospheric circulation anomalies among models. Thus, the spread of circulation changes in response to global warming across climate models leads to a diversity of responses in the

80   hydrological cycle.

Proxy data indicate that the mid-Pliocene (~3 million years ago) was one of the most recent warm periods with CO_2 levels similar to the current anthropogenically elevated value of 400 ppm and can be considered an analog for future climate change (Dowsett et al., 2012; Burke et al., 2018; Tierney et al., 2019). Pliocene Model Intercomparison Project Phase 1 (PlioMIP1) simulations have been used to investigate how the climate system responded to mid-Pliocene boundary

85   conditions, including elevated atmospheric CO_2 concentrations. These past warm climate simulations exhibit many similarities with future climate projections. For example, one robust characteristic is increased temperature from 1.8 to 3.6℃ during the Pliocene compared with the preindustrial period (PI) (Haywood et al., 2013), with Arctic amplification in response to a significant sea-ice extent decline (Howell et al., 2016; Zheng et al., 2019). These features could have reduced the meridional surface temperature gradient, inducing weaker tropical circulation (i.e., local Hadley circulation) during the

90   Pliocene (Sun et al., 2013a; Li et al., 2015; Corvec and Fletcher, 2017). Additionally, some studies have suggested a weakened zonal sea surface temperature (SST) gradient in the Pacific during the Pliocene (Wara et al., 2005; Scroxton et al., 2011), which would have favored weaker Walker circulation. These features could have induced large-scale changes in Pliocene hydroclimate. Using a climate simulation that captures the warming patterns seen in Early Pliocene sea surface temperature proxies, Burls and Fedorov (2017) suggested that the dynamic process might play a key role in driving wetter

95   subtropics due to this weaker tropical circulation during the Early Pliocene warm climate compared with the future climate.

Although PlioMIP1 can reproduce similar patterns of the change in surface temperature to the reconstructed SST, models cannot capture the magnitude of warming at higher latitudes. For example, Dowsett et al. (2012) indicated that the ensemble of PlioMIP1 models underestimates the warming in the North Atlantic compared with the reconstructed SST. This might be induced by the uncertainties in PlioMIP1, including the uncertainty in atmospheric CO_2 concentrations (Salzmann

100 et al., 2013; Howell et al., 2016; Samakinwa, 2018) and paleogeography and bathymetry (Otto-Bliesner et al., 2016; Feng et al., 2017; Samakinwa, 2018). In PlioMIP2 models, the boundary conditions have been updated using the new version of the U.S. Geological Survey PRISM4 dataset (Dowsett et al., 2016; Haywood et al., 2016). These include the closed Canadian Archipelago and Bering Strait and a reduced Greenland ice sheet relative to PlioMIP1. In addition, PlioMIP2 focuses on a specific time slice during the mid-Pliocene at approximately 3.025 Ma, which could reduce the uncertainties in

105 reconstructions (Mcclymont et al., 2020). Researchers have been investigating the mid-Pliocene climate by using PlioMIP2, including Arctic warming (De Nooijer et al., 2020), Atlantic meridional overturning circulation (Zhang et al., 2021b),

climate sensitivity (Haywood et al., 2020), global monsoons (Zhang et al., 2021a), and subtropical rainfall changes (Pontes et al., 2020). However, it is difficult to distinguish the relative impact of the Hadley circulation and Walker circulation on Pliocene hydrological cycling at low latitudes. Fortunately, the three-pattern decomposition of global atmospheric circulation (3P-DGAC; Hu et al., 2017, 2018b, c) method can help us to decompose atmospheric circulation into zonal (i.e., local Walker circulation) and meridional (i.e., local Hadley circulation) circulation at low latitudes. We apply this method to develop moisture budget analyses, which might provide some insight into the mechanisms of hydrological cycling during the mid-Pliocene.

This paper is in the framework of updated PlioMIP2 models to quantitatively distinguish the relative contribution from zonal and meridional circulation anomalies to hydrological cycle changes. In the following section, we first introduce the PlioMIP2 models and moisture budget decomposition. We then evaluate the simulated large-scale hydroclimate cycle response within the PlioMIP2 ensemble in section 3. Section 4 provides each moisture budget component's relative contribution to investigate the potential mechanisms driving the simulated changes in the mid-Pliocene hydrological cycle. The corresponding mechanisms are discussed in section 5. The last section contains the conclusion and discussion.

2 Data and analytical methods

2.1 Climate model simulations

In this study, we use the simulations from 13 models participating in PlioMIP2 (Table 1). All models include a preindustrial (PI) simulation and a Pliocene climate simulation. To calculate the ensemble mean, we interpolate all data onto a common grid with a 1°×1° resolution using bilinear interpolation.

140

Table 1: PlioMIP2 models used in this study

Model name	Institute	PlioMIP2 reference
1. CESM2	NCAR	Feng et al. (2020)
2. COSMOS	Alfred Wegener Institute	Samakinwa et al. (2020)
		Stepanek et al. (2020)
3. EC-Earth3-LR	Stockholm University	Zhang et al. (2021a)
4. HadCM3	Hadley Centre for Climate Prediction and Research/Met Office UK	Hunter et al. (2019)
5. GISS-E2-1-G	NASA/GISS	Chandler et al. (in prep.)
6. IPSL-CM6A-LR	Laboratoire des Sciences du Climat et de l'Environnement (LSCE)	Lurton et al. (2020)
7. CCSM4-UofT	University of Toronto, Canada	Chandan and Peltier (2017)
8. NorESM1-F	NORCE Norwegian Research Centre, Bjerknes Centre for Climate Research, Bergen, Norway	Li et al. (2020)
9. NorESM-L	NORCE Norwegian Research Centre, Bjerknes Centre for Climate Research, Bergen, Norway	Li et al. (2020)
10. CCSM4-Utrecht	IMAU, Utrecht University	Baatsen et al. (2021), in prep
11. HadGEM3	Hadley Centre for Climate Prediction and Research/Met Office UK	Williams et al. (2021), in prep
12. CCSM4	NCAR	Feng et al. (2020)
13. CESM1.2	NCAR	Feng et al. (2020)

2.2 Development of moisture budget decomposition

To examine the changes in precipitation (P) minus evaporation (E) in the PlioMIP2 mid-Pliocene experiments relative to
145 their respective PI simulation, we decompose the moisture budget equation based on Seager et al. (2010), i.e.,

$$\delta(\overline{P}-\overline{E}) \approx -\underbrace{\frac{1}{\rho_w g}\nabla\cdot\int_0^{p_s}(\overline{V_0}\,\delta\overline{q})dp}_{\delta TH} -\underbrace{\frac{1}{\rho_w g}\nabla\cdot\int_0^{p_s}(\overline{q}\,\delta\overline{V_0})dp}_{\delta MCD} + R \qquad (1)$$

Here, g is gravity, ρ_w is the density of water, $\vec{V}$ is the horizontal wind, and q is the specific humidity. $\delta(\cdot)$ is the annual mean difference of variables between the warmer climate state (mid-Pliocene) and PI simulation. Subscript 0 represents the variables in the PI simulation. In the warmer climate, the change in P minus E [PmE, the left-hand side of Eq.

150 (1)] is balanced by the thermodynamic (δTH, induced by increased specific humidity) and dynamic (δMCD, induced by circulation anomalies) contributions and residual term (R, which is mainly involved in the contributions from high-frequency variability of transient eddies, nonlinear effects and surface boundary terms).

Since we are interested in understanding the relative contribution from zonal circulation (i.e., local Walker circulation) changes and meridional circulation (i.e., local Hadley circulation) anomalies to the changes in PmE in a warmer

155 climate, we further apply the three-pattern decomposition of global atmospheric circulation (3P-DGAC; Hu et al., 2017, 2018b, c) method in this study. The horizontal, meridional, and zonal circulations that can be viewed as the global generalization of the Rossby wave in the middle-high latitudes and the Hadley and Walker circulations in the low latitudes are defined to decompose the global atmospheric circulation into a superposition of the horizontal, meridional, and zonal circulations by using the 3P-DGAC method.

160 Based on the essential features of the Rossby, Hadley and Walker circulations, Hu et al. (2017) defined the 3D horizontal circulation $\vec{V}_R$, meridional circulation $\vec{V}_M$ and zonal circulation $\vec{V}_Z$ in the spherical σ-coordinate system as follows:

$$
\begin{cases}
\vec{V}_R(\lambda,\theta,\sigma) = u_R(\lambda,\theta,\sigma)\vec{i} + v_R(\lambda,\theta,\sigma)\vec{j}, \\
\vec{V}_M(\lambda,\theta,\sigma) = v_M(\lambda,\theta,\sigma)\vec{j} + \dot{\sigma}_M(\lambda,\theta,\sigma)\vec{k}, \\
\vec{V}_Z(\lambda,\theta,\sigma) = u_Z(\lambda,\theta,\sigma)\vec{i} + \dot{\sigma}_Z(\lambda,\theta,\sigma)\vec{k}.
\end{cases}
\tag{2}
$$

and the following continuity equations are satisfied:

$$
\begin{cases}
\dfrac{1}{\sin\theta}\dfrac{\partial u_R}{\partial\lambda} + \dfrac{1}{\sin\theta}\dfrac{\partial(\sin\theta v_R)}{\partial\theta} = 0, \\[2mm]
\dfrac{1}{\sin\theta}\dfrac{\partial(\sin\theta v_M)}{\partial\theta} + \dfrac{\partial\dot{\sigma}_M}{\partial\sigma} = 0, \\[2mm]
\dfrac{1}{\sin\theta}\dfrac{\partial u_Z}{\partial\lambda} + \dfrac{\partial\dot{\sigma}_Z}{\partial\sigma} = 0.
\end{cases}
\tag{3}
$$

165

Equation (3) is the sufficient condition that the components of $\vec{V}_R$, $\vec{V}_M$ and $\vec{V}_Z$ can be represented by the stream functions $R(\lambda,\theta,\sigma)$, $H(\lambda,\theta,\sigma)$ and $W(\lambda,\theta,\sigma)$, respectively, as follows:

$$\begin{cases} u_R = -\dfrac{\partial R}{\partial \theta}, v_R = \dfrac{1}{\sin \theta} \dfrac{\partial R}{\partial \lambda}, \\[2mm] v_M = -\dfrac{\partial H}{\partial \sigma}, \dot{\sigma}_M = \dfrac{1}{\sin \theta} \dfrac{\partial (\sin \theta H)}{\partial \theta}, \\[2mm] u_Z = \dfrac{\partial W}{\partial \sigma}, \dot{\sigma}_Z = -\dfrac{1}{\sin \theta} \dfrac{\partial W}{\partial \lambda}. \end{cases} \tag{4}$$

Because three-pattern circulations (horizontal, meridional and zonal circulations) exist in both the low and middle-

170 high latitudes, the global atmospheric circulation can be expressed as the superposition of the horizontal, meridional and zonal circulations, that is,

$$\vec{V} = \vec{V}_M + \vec{V}_Z + \vec{V}_R, \tag{5}$$

with the following components:

$$\begin{cases} u = u_Z + u_R = \dfrac{\partial W}{\partial \sigma} - \dfrac{\partial R}{\partial \theta}, \\[2mm] v = v_R + v_M = \dfrac{1}{\sin \theta} \dfrac{\partial R}{\partial \lambda} - \dfrac{\partial H}{\partial \sigma}, \\[2mm] \dot{\sigma} = \dot{\sigma}_M + \dot{\sigma}_Z = \dfrac{1}{\sin \theta} \dfrac{\partial (\sin \theta H)}{\partial \theta} - \dfrac{1}{\sin \theta} \dfrac{\partial W}{\partial \lambda}. \end{cases} \tag{6}$$

175 Equation (5) or (6) is called the three-pattern decomposition model.

In contrast to the traditional two-dimensional decomposition of the atmospheric motion into vortex and divergent parts, the continuity Eq. (5) cannot guarantee the uniqueness of the stream functions $R(\lambda, \theta, \sigma)$, $H(\lambda, \theta, \sigma)$ and $W(\lambda, \theta, \sigma)$ because the three-pattern circulations $\vec{V}_R$, $\vec{V}_M$ and $\vec{V}_Z$ have three spatial dimensions, respectively (Hu et al., 2017, 2018a, b). The following restriction condition is needed to pick up the correct decomposition (Theorems 1 and 2 in Hu

180 et al., 2018a):

$$\frac{1}{\sin \theta} \frac{\partial H}{\partial \lambda} + \frac{1}{\sin \theta} \frac{\partial (W \sin \theta)}{\partial \theta} + \frac{\partial R}{\partial \sigma} = 0. \tag{7}$$

Equation (7) guarantees both the uniqueness of the stream functions R, H and W and the physical rationality of the 3P-DGAC method.

Using the 3P-DGAC method, we can rephrase the moisture budget in Eq. (1) to involve the contributions from

185 zonal and meridional circulation. Here, we neglect the relatively smaller terms at low latitudes, including transient eddies,

nonlinear effects and surface boundary terms. Thus, we mainly explore the contributions from δTH and δMCD to changes in PmE in this study. Then, the δTH and δMCD can be rewritten as:

$$\delta TH = \underbrace{\underbrace{-\frac{1}{\rho g}\int_0^{p_s}\delta q\nabla\cdot\vec{V}_{R0}dp}_{\delta TH_{D\_R}}\underbrace{-\frac{1}{\rho g}\int_0^{p_s}\delta q\nabla\cdot\vec{V}_{Z0}dp}_{\delta TH_{D\_Z}}\underbrace{-\frac{1}{\rho g}\int_0^{p_s}\delta q\nabla\cdot\vec{V}_{M0}dp}_{\delta TH_{D\_M}}}_{\Delta\delta TH_D}$$
$$\underbrace{\underbrace{-\frac{1}{\rho g}\int_0^{p_s}\vec{V}_{R0}\cdot\nabla\delta q dp}_{\delta TH_{A\_R}}\underbrace{-\frac{1}{\rho g}\int_0^{p_s}\vec{V}_{Z0}\cdot\nabla\delta q dp}_{\delta TH_{A\_Z}}\underbrace{-\frac{1}{\rho g}\int_0^{p_s}\vec{V}_{M0}\cdot\nabla\delta q dp}_{\delta TH_{A\_M}}}_{\delta TH_A}$$

(8)

$$\delta MCD = \underbrace{\underbrace{-\frac{1}{\rho g}\int_0^{p_s}q_0\nabla\cdot\delta\vec{V}_R dp}_{\delta MCD_{D\_R}}\underbrace{-\frac{1}{\rho g}\int_0^{p_s}q_0\nabla\cdot\delta\vec{V}_Z dp}_{\delta MCD_{D\_Z}}\underbrace{-\frac{1}{\rho g}\int_0^{p_s}q_0\nabla\cdot\delta\vec{V}_M dp}_{\delta MCD_{D\_M}}}_{\delta MCD_D}$$
$$\underbrace{\underbrace{-\frac{1}{\rho g}\int_0^{p_s}\delta\vec{V}_R\cdot\nabla q_0 dp}_{\delta MCD_{A\_R}}\underbrace{-\frac{1}{\rho g}\int_0^{p_s}\delta\vec{V}_Z\cdot\nabla q_0 dp}_{\delta MCD_{A\_Z}}\underbrace{-\frac{1}{\rho g}\int_0^{p_s}\delta\vec{V}_M\cdot\nabla q_0 dp}_{\delta MCD_{A\_M}}}_{\delta MCD_A}$$

(9)

where subscripts D and A represent the terms that are related to divergence and moisture advection, respectively. In addition, the subscripts R, Z, and M indicate the terms that are related to the horizontal, zonal and meridional circulations, respectively. Note that $\vec{V}_R$ represents the horizontal vortex winds, which are nondivergent, which indicates that the terms that are related to the divergence/convergence of $\vec{V}_R$ (i.e., δTH_{D_R} and δMCD_{D_R}) are zero. These terms can be clearly seen in Figs. 3(h) and 4(h). In addition, we ignore these two terms in this study.

3 Changes in precipitation minus evaporation (PmE) in the PlioMIP2 models

The last 100 years of individual PlioMIP2 simulations are used to calculate the multimodel mean (MMM) PmE in Fig. 1 and individual PlioMIP2 models in Fig. 2.

Figure 1(a) shows that most subtropical regions experience reduced PmE in the mid-Pliocene simulations with respect to the PI simulations, including the subtropical Pacific and subtropical Atlantic in both hemispheres and the subtropical Indian Ocean in the Southern Hemisphere (SH). There is also drying over the South Pacific convergence zone (SPCZ), except in the GISS-E2-1-G, COSMOS and HadGEM3 models (Fig. 2), consistent with other studies evaluating the hydrological cycle response within the PlioMIP2 simulations (Pontes et al., 2020). In contrast, the increased MMM PmE is

located in the deep tropics [i.e., Pacific intertropical convergence zone (ITCZ), Maritime Continent, and North Indian Ocean], as well as at mid-high latitudes (Fig. 1(a)). However, some models, i.e., the CESM2, GISS-E2-1-G, COSMOS and HadGEM3 models, show a drier Maritime Continent (Fig. 2), which might be related to the changes in Walker circulation (we will discuss this latter in Section 5.3). In addition, the North African and Southeast Asian monsoon regions also show significant moistening signals, which are consistent with faunal remains and palynological transfer functions (Sanyal et al., 2004; Trauth et al., 2007; Xie et al., 2012), as well as with other modeling studies (Zhang et al., 2019a; Li et al., 2020; Feng et al., 2021). This change over Southeast Asia is robust among PlioMIP2 models, and only the COSMOS model shows a drier change over East Asia (Fig. 2(e)). Furthermore, the MMM PmE changes over Southeast Asia are mainly focused on the summer time (not shown), suggesting a consequence of strengthened East Asian summer monsoon circulation (Salzmann et al., 2008; Wan et al., 2010; Yan et al., 2012; Zhang et al., 2013; Li et al., 2018; Lu et al., 2021). Note that the mid- to high-latitude North Atlantic becomes drier (Fig. 1), and this change might be caused by the simulated largely increased SST in the North Atlantic (Fig. 5(b)).

Generally, the response of the hydrological cycle during the mid-Pliocene generally shows a wet-regions-getting-wetter-and-dry-regions-getting-drier pattern, especially over the ocean. These features are apparent in the zonal average of the PmE change (Fig. 1(b)), except in the GISS-E2-1-G model (Fig. 2(f)). The tropical regions become wetter, and subtropical regions become drier, which are similar to the results from future high-CO_2 scenario experiments (Chou et al., 2009).
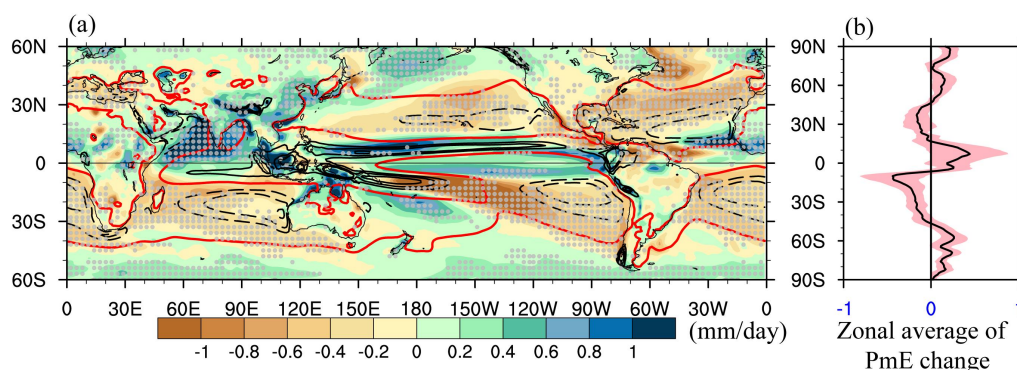
Figure 1: (a) Changes in multimodel mean (MMM) PmE for the mid-Pliocene compared with the PI simulation (shading), overlaid by the climatological MMM PmE of the PI simulation (for the contours, a solid line indicates positive values and a dashed line indicates negative values). The red solid curves represent the zero value. (b) The zonal average of the change in PmE, where the shading indicates 1 standard deviation of individual models departing from the MMM mean. Stippling (left) indicates regions where at least 10 of 12 simulations in the model group agree on the sign of the ensemble mean. Units: mm·day^{-1}.
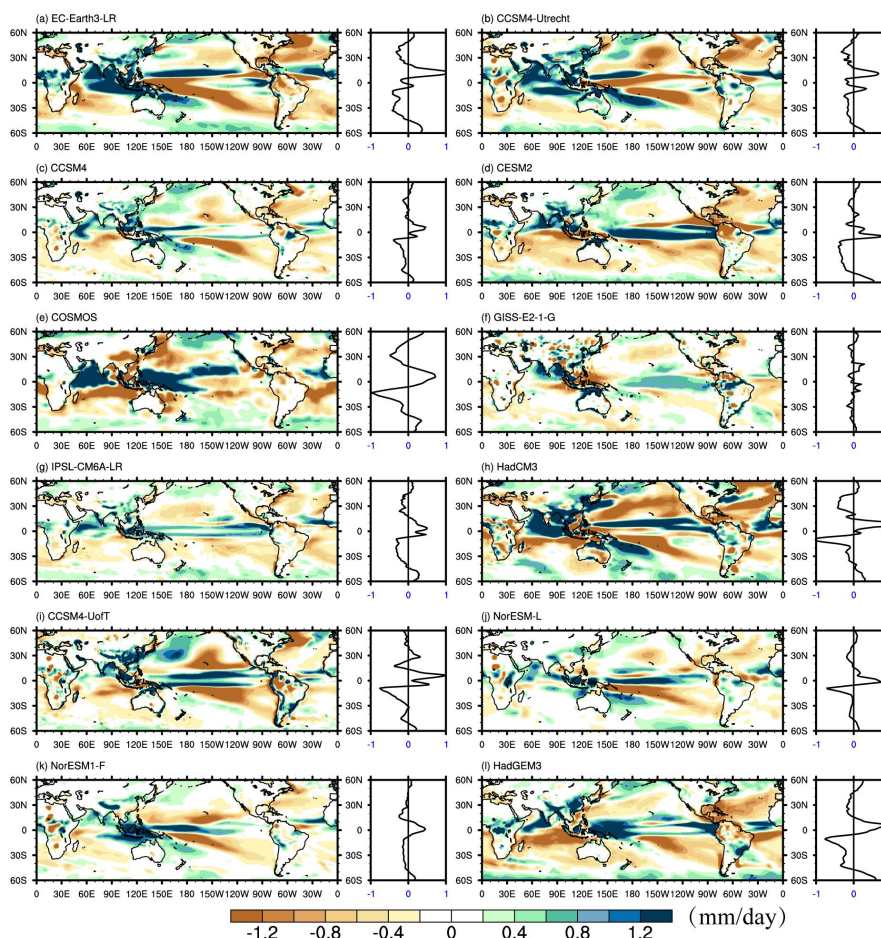
Figure 2: The simulated PmE changes in individual PlioMIP2 models. The zonal average of the PmE changes in each model is shown on the right. Units: mm·day⁻¹.

4 Thermodynamic and dynamic contributions to changes in PmE

230 Moisture budget analyses are conducted to shed light on the mechanisms driving the changes in PmE during the mid-Pliocene. Based on this decomposition, the changes in PmE are mainly influenced by the change in humidity with unaltered atmospheric circulation (called the thermodynamic term, δTH) and change in atmospheric circulation with no change in humidity (called the dynamic term, δMCD) at low latitudes. The thermodynamic term (δTH) and its decomposition are plotted in Fig. 3. It is clear that δTH captures the main features of hydrological cycle change (Figs. 3(a) vs 1(a)). That is, the

235 positive and negative contributions over the already convergent (i.e., ITCZ and SPCZ) and divergent (subsidence of local Hadley circulation) regions, respectively. This term does not alter the spatial distribution of climatological PmE (contours in Fig. 1(a)) but amplifies the intensity of the existing pattern of PmE, reflecting the wet-getting-wetter-and-dry-getting-drier

mechanisms (Held and Soden, 2006). The results are consistent with future global warming scenarios (Chou et al., 2009; Wang et al., 2012; Li et al., 2013).

240   From the perspective of global atmospheric circulation, previous studies have indicated that global atmospheric circulation can be decomposed into a superposition of horizontal, meridional, and zonal circulations (Hu et al., 2017, 2018a, b). δTH is further decomposed by using the 3P-DGAC method (Fig. 3(c)-(k)). The estimated δTH in Fig. 3(b), calculated by the sum of the right-hand side in Eq. (8) of the 3P-DGAC decomposition method shows a similar distribution to the δTH field shown in Fig. 3(a) with a pattern correlation coefficient (PCC) of 0.80. This result indicates that the decomposition is

245 representative. At low latitudes, the δTH mainly comes from terms that are related to climate mean meridional and zonal circulation (Fig. 3(c) and (d)); while at mid-high latitudes, the δTH mainly comes from horizontal circulation (Fig. 3(e)). It is clear that the thermodynamic changes associated with meridional circulation can explain the large portion of δTH (PCC of 0.9) at low latitudes, which is caused by increased specific humidity within the divergence of climate mean meridional circulation (δTH_{D_M} ; Fig. 3(f)). The zonal circulation can also explain δTH to some extent, with a positive contribution

250 mainly over Maritime Continent extending eastward to the equatorial central Pacific and eastern coast of North/South America, and a negative contribution over the eastern Pacific extending from the western Indian Ocean to the Greater Horn of Africa and the eastern tropical Atlantic (Fig. 3(d)). These changes associated with zonal circulation are linked to the increased specific humidity with unaltered divergence of the mean zonal circulation (δTH_{D_Z} ; Fig. 3(g)). At mid-high latitudes, the δTH induced by climate mean horizontal circulation is caused by changes in moisture advection (Fig. 3(k)).

255
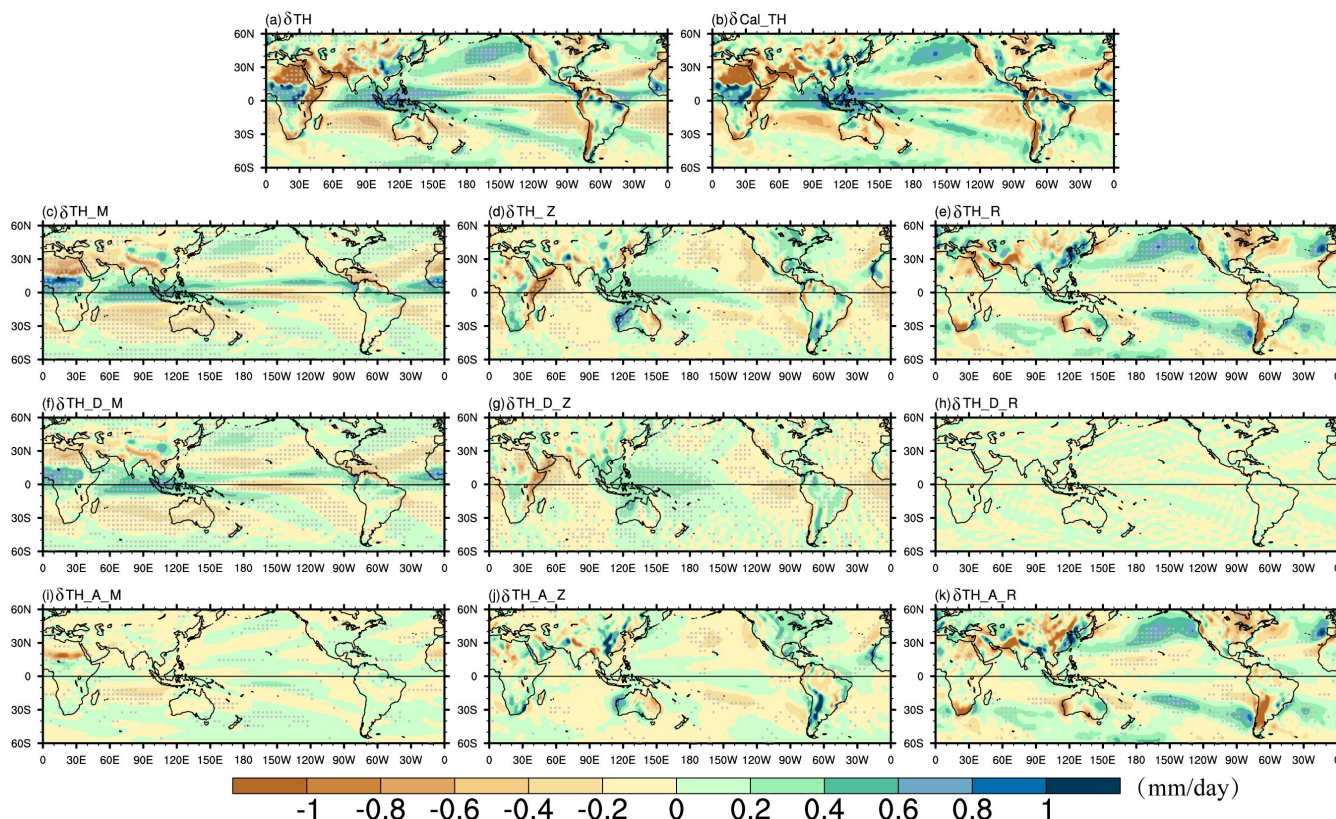
Figure 3: The annual mean changes in the moisture budget components of the mid-Pliocene minus PI control of the PlioMIP2 multimodel mean, which reflect (a) the thermodynamic term and (b) the estimated change in the thermodynamic term [calculated by the sum of the right-hand side terms in Eq. (8) of the 3P-DGAC decomposition method]. The contributions to the change in the thermodynamic: the thermodynamic term induced by the climate mean (c) meridional, (d) zonal and (e) horizontal circulations.

260 **The corresponding changes in (f-h) and (i-k) are the terms in (c-d) the component related to divergent mean flow and change in moisture advection, respectively. Stippling indicates regions where at least 10 of 13 simulations in the model group agree on the sign of the ensemble mean. Units: mm·day⁻¹.**

It is evident that the δTH component does not describe the full contribution to the changes in PmE, especially over

265 the North African and Southeast Asian monsoon regions, SPCZ and North Indian Ocean, where we must consider the

dynamic effect. The dynamic effect (δMCD), reflecting the impact of circulation changes, partially offsets the δTH at low

latitudes (Fig. 4(a)). In particular, δMCD reduces PmE in the deep tropics, i.e., the ITCZ, SPCZ and Maritime Continent. In

contrast, δMCD can moisten subtropical regions, especially over the subtropical eastern Pacific, southern Indian Ocean and

Atlantic Ocean of both hemispheres. Compared with δTH, the overwhelming contribution from δMCD to changes in PmE

270 lies adjacent to the North Indian Ocean, SPCZ and the North African and Southeast Asian monsoon regions (Fig. 4(a)).

The estimated δMCD in Fig. 4(b), calculated by the sum of the right-hand side terms in Eq. (9) of the 3P-DGAC

decomposition method, is consistent with the δMCD in Fig. 4(a) with a PCC of 0.93. This result indicates that the

decomposition is representative. The anomalous divergence of the meridional circulation component (δMCD_{D_M}) appears

to dry the southern part of the deep tropics but moisten its northern part, which is associated with the northward shift of the

275 ITCZ (Fig. 7(c)). In particular, the northward shift of the ITCZ is clear from 150°E to the east in the Pacific (Fig. 4(f)). In

addition, the component contributes a large portion to enhance PmE over the North African and Southeast Asian monsoon

regions. However, the tropical southern Pacific is even more complicated. There is a tendency to reduce PmE via the

δMCD_{D_M} term but increase its southern part in the tropical southern Pacific. A previous study suggested that these

changes in PmE followed the southward shift of the SPCZ, which was mainly modulated by the intensified and westward

280 shift of the South Pacific subtropical high for the mid-Pliocene compared with the PI simulation (Pontes et al., 2020). For the

adjacent north Indian Ocean, the convergence of zonal circulation anomalies (δMCD_{D_Z}) is the first-order contribution to

strengthen the dynamic effect and hence enhance the PmE (Fig. 4(g)).
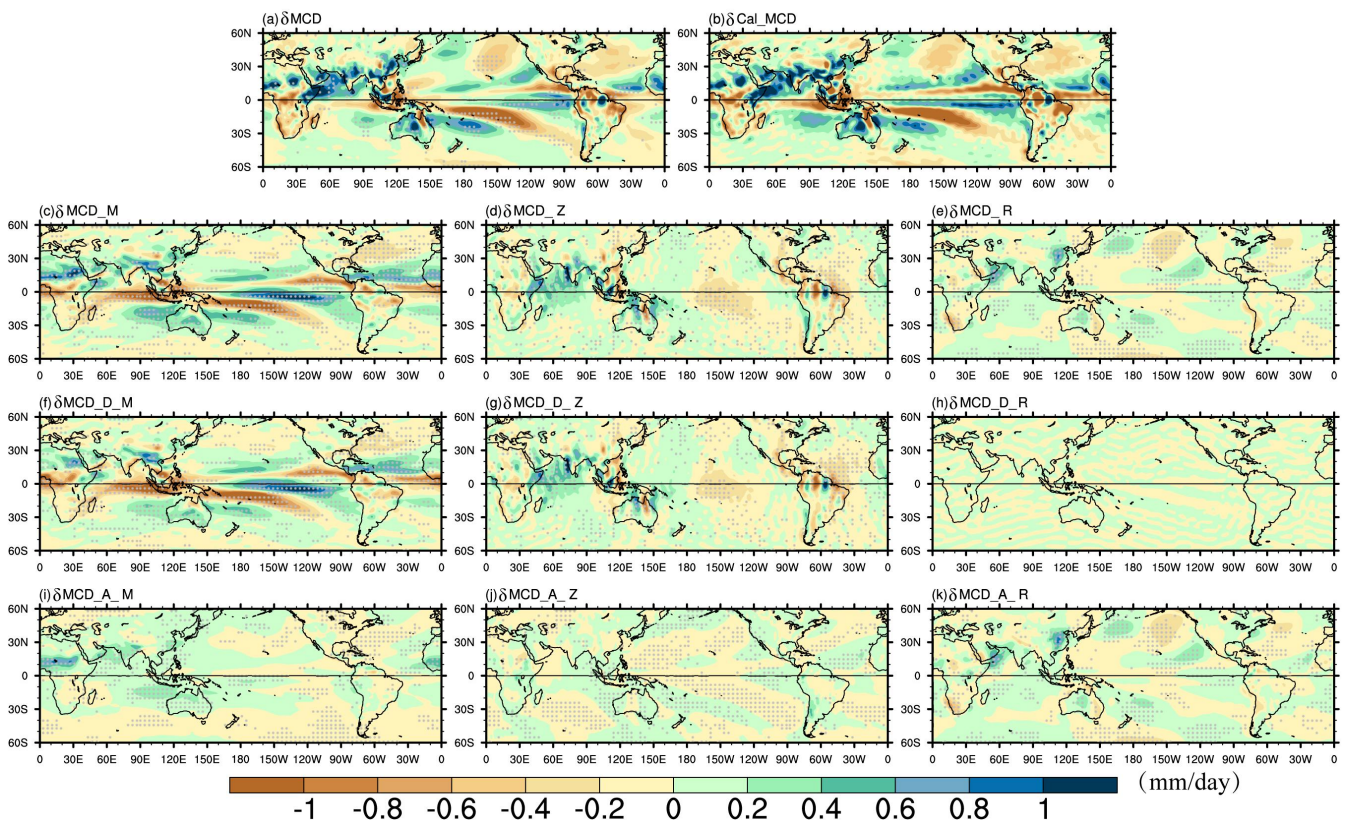
Figure 4: The annual mean changes in the moisture budget components of the mid-Pliocene minus PI control of the PlioMIP2
285 **multimodel mean, which reflect (a) the dynamic term and (b) the estimated dynamic term [calculated by the sum of the right-hand side terms in Eq. (9) of the 3P-DGAC decomposition method]. The contributions to the dynamic: the dynamic term induced by the anomalous (c) meridional, (c) zonal, and (d) horizontal circulations. The corresponding changes in (f-h) and (i-k) are the terms in (c-d) the component related to divergent mean flow and change in moisture advection, respectively. Stippling indicates regions where at least 10 of 13 simulations in the model group agree on the sign of the ensemble mean. Units: mm·day^{-1}.**

290

    In summary, the thermodynamic term induced by the divergence of the mean meridional circulation is the dominant process driving changes in PmE at low latitudes (Fig. 3(f)). However, the dynamic term partially offsets δTH, especially over the ITCZ, SPCZ and Maritime Continent, via changes in the divergence of meridional circulation. Even the dynamic term overwhelmingly contributes to the increased changes in PmE over North African and Southeast Asian monsoon regions

295 and the North Indian Ocean. Note that the former two are mainly caused by meridional circulation anomalies, but the latter is dominated by zonal circulation anomalies.

    We further decompose the meridional moisture transport into terms that reflect the changes in specific humidity (meridional moisture transport induced by the thermodynamic effect; MMTT) and circulation (meridional moisture transport induced by the dynamic effect; MMTD) in Fig. 5(a). As expected, all models show that the MMTT is responsible for the

300 wetter tropics and drier subtropics in the mid-Pliocene simulation, indicating a dry-gets-drier-and-wet-gets-wetter mechanism. These features are robust among models and are associated with the increased specific humidity combined with the mean meridional circulation from the PI control (Fig. 5(b)), as mentioned above. This is because the zonal-mean wind depicts southerly (northerly) wind between the equator and subtropical SH (Northern Hemisphere; NH) for the climate mean meridional circulation in the PI simulations. When the climatological wind is combined with increased specific humidity in

305 the low-level troposphere (Fig. 6(b)), more moisture is transported from the subtropics to the tropics, resulting in drier subtropics and wetter tropics. In contrast, the MMTD shows a large spread across PlioMIP2 models. On average, the anomalous MMTD appears to weaken thermodynamic contributions in the subtropical NH but strengthen it in the subtropical SH via meridional circulation anomalies (Fig. 5(c)). This indicates that the changes in MMTD favor the transport of more (less) moisture from the tropics to the NH (SH) subtropics, which is caused by the northward shift of the meridional

310 circulation (as detailed further in section 5.2). The equatorward moisture transport anomalies of SH's dynamic component are due to anomalous southerly winds in the subtropical southern Pacific (Fig. 8). This feature acts to dry the SPCZ and moisten the south SPCZ and the equatorial central-eastern Pacific (Fig. 4(f)).
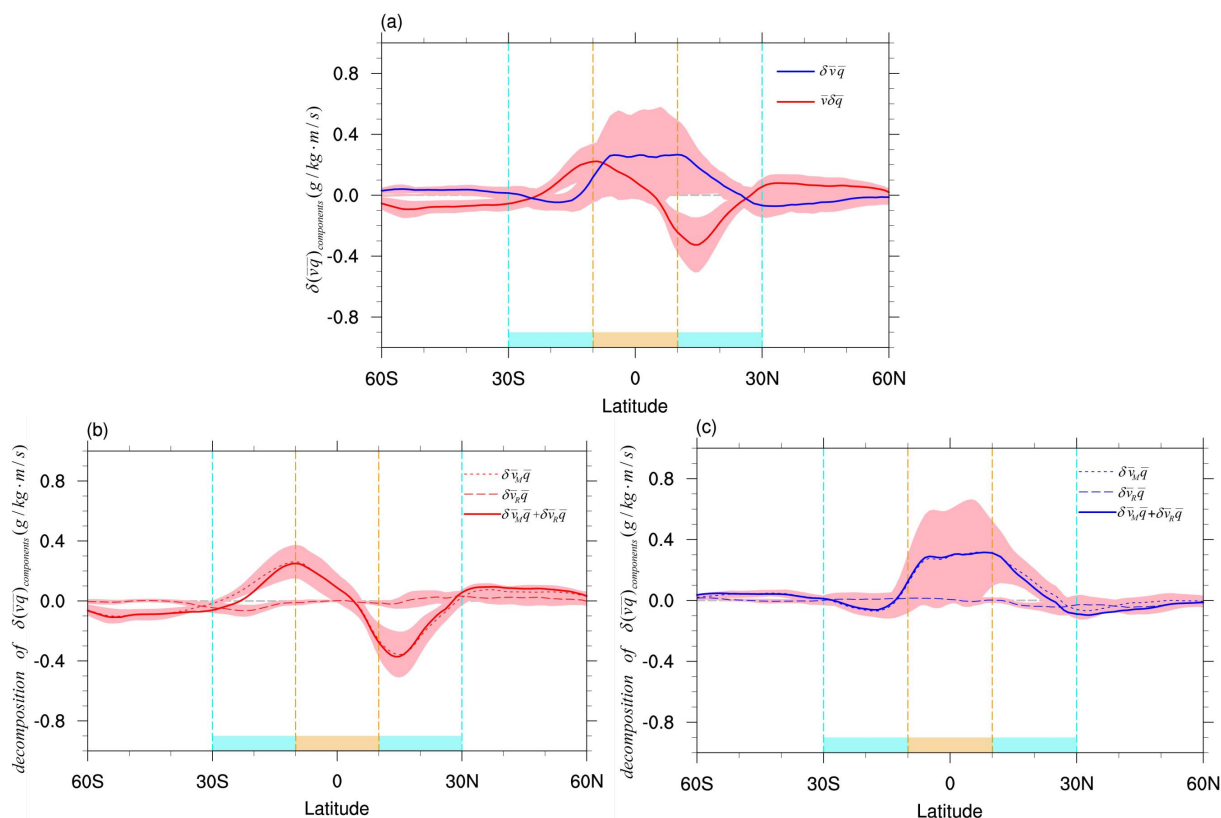
Figure 5: (a) The time-mean meridional moisture transport anomalies induced by thermodynamic and dynamic effects for the mid-Pliocene compared with PI simulations. (b) and (c) are thermodynamic and dynamic terms in (a) that are induced by the meridional wind $\vec{V}_M$ and $\vec{V}_R$ decomposed from the 3P-DGAC method, respectively. Here, the tropical region is defined as the region between 10°S and 10°N (marked as a green band), while the subtropical region refers to 10-30° N and 10-30° S (marked as an orange band). The shading indicates 1 standard deviation of individual models departing from the MMM. Units: g•kg⁻¹•m•s⁻¹.

5 Mechanisms for the changes in moisture budget components

Thus far, we have shown that the anomalous hydroclimate within the mid-Pliocene simulations involves anomalies of both thermodynamic and dynamic effects at low latitudes. In this section, we further examine the corresponding mechanisms in turn.

5.1 Changes in specific humidity

Figure 6(a) shows the changes in MMM SST superimposed on the reconstructed SST anomalies (Mcclymont et al., 2020). In the MMM, SSTs range from between 1 and 6°C warmer in the mid-Pliocene simulations than in the PI simulations. The most pronounced SST warming is located in the Southern Ocean, North Atlantic, and North Pacific, consistent with current studies (Haywood et al., 2020; Williams et al., 2021). Following the Clausius-Clapeyron relationship, this global warming

increases specific humidity in the low-level troposphere (Fig. 5(b)). On the other hand, the sinking branch of meridional

circulation in the control climate is located in subtropical regions, showing divergent circulation $\nabla \cdot \vec{V} > 0$ in the low-level

330   troposphere. And the contrary applies for the regions of deep tropics, i.e., ITCZ and SPCZ. These two factors contribute the

δTH_{D_M} term (i.e., $-\dfrac{1}{\rho g}\int_{0}^{p_s} \delta q \nabla \cdot \vec{V}_{M0}\,dp$) to the thermodynamic effect (Figure 3f) and hence changes in PmE.

Although the δTH_{D_M} term is the first-order to control the thermodynamic effect in most regions, δTH_{D_Z} term

contributes to the thermodynamic effect to some extent, especially over the adjacent north Indian Ocean. The climate mean

zonal circulation characterizes ascending in the tropical western Pacific, tropical African and tropical southern American

335   regions, favoring convergent circulation (i.e., $-\nabla \cdot \vec{V}_{Z_0} > 0$) there (Fig. 6(d); Hastenrath, 1991; Peixoto and Oort, 1992).

With increased specific humidity ($\delta q > 0$) under a warmer climate, the δTH_{D_Z} term (i.e., $-\dfrac{1}{\rho g}\int_{0}^{p_s} \delta q \nabla \cdot \vec{V}_{Z0}\,dp$)

shows positive contribution and hence increase PmE in these regions (Figure 3g). In the contrary, the δTH_{D_Z} favors to

decrease PmE over the western Indian Ocean, eastern Pacific and tropical Atlantic (Figure 3g), where the climate mean zonal

circulation is divergent (Figure 6d).
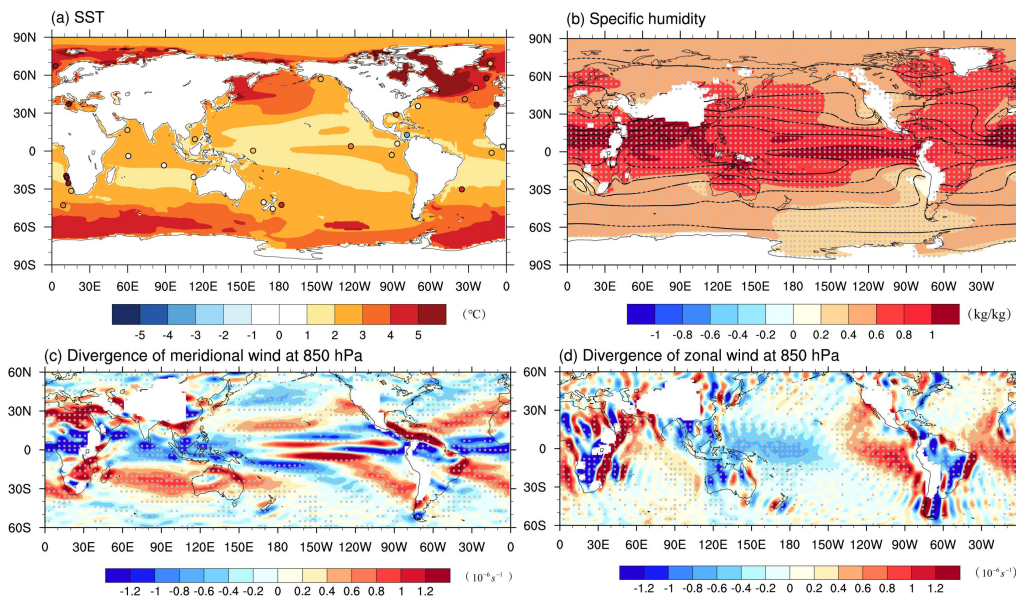
340

Figure 6: Change in (a) MMM SST (shading, unit: ℃), (b) specific humidity (shading, unit: kg•kg⁻¹) overlaid by its climate mean for PI simulation. (c) and (d) show the MMM divergence of meridional $\vec{V}_M$ and zonal wind $\vec{V}_Z$ fields decomposed from the 3P-DGAC method at the 850 hPa level for PI simulation (unit: 10⁻⁶ s⁻¹). The circles in (a) are the anomalies of reconstructed SST from

the alkenone-derived $U_{37}^{K'}$ index (Prahl and Wakeham, 1987) and foraminifera calcite Mg/Ca (Delaney et al., 1985). **Stippling in**
345 **(b-d) indicates regions where at least 10 of 13 simulations in the model group agree on the sign of the ensemble mean.**

5.2 Response in meridional circulation

In section 4, we have demonstrated that the primary dynamic contribution to changes in PmE is a consequence of anomalous meridional circulation (δMCD_{D_M} term). Figure 7(a) shows the annual mean mass stream function (MSF) of meridional circulation for PI simulation (contours), which is similar to present-day meridional circulation (Cheng et al., 2020). During
350 the mid-Pliocene, the meridional circulation changes are characterized by enhanced meridional circulation in the SH tropics and weakened meridional circulation in the NH tropics (shading in Fig. 7), which is caused by the northward shift of meridional circulation in the SH, as indicated in our later discussion. To quantify meridional circulation changes, we further calculated the intensity in Fig. 7(b). The intensity is defined as the maximum of the absolute average MSF between 200 hPa and 925 hPa in the range of 30°S to 30°N (Oort and Yienger, 1996) in Fig. 7(a). Models simulate a consistently weakened
355 meridional circulation intensity in the NH and a slightly strengthened intensity in the SH (Fig. 7(b)), which is related to the hemispheric asymmetry of the atmospheric energy budget (Feng et al., 2020).

As a result, meridional circulation anomalies could induce divergent/convergent circulation anomalies in the low-level troposphere (Fig. 8). The weakened local meridional circulation leads to anomalous southerly winds spanning northeastern South America eastward to the northwestern Pacific region. These meridional circulation anomalies induce the
360 anomalous divergence (convergence) of circulation over the Indo-Pacific warm pool (adjacent to subtropic regions), resulting in a negative (positive) contribution from δMCD_{D_M} (Figs. 8 vs 4(f)). In fact, this anomalous meridional circulation is closely related to the strengthened Asian summer monsoon (not shown), consistent with previous studies (Zhang et al., 2013; Prescott et al., 2019). In addition, anomalous northerly winds exist in the western tropical Pacific, but southerly winds are located in the central Pacific. These circulation anomalies could induce δMCD_{D_M}, which favors
365 moistening of the equatorial central Pacific and southern part of the SPCZ region but dries the SPCZ (Fig. 4(f)). Previous studies have indicated that these circulation anomalies are caused by the southward shift of the SPCZ, which is mainly modulated by the intensified and westward shift of the South Pacific subtropical high for the mid-Pliocene compared with the PI simulation (Pontes et al., 2020).

One question arises as to what causes the meridional circulation changes in mid-Pliocene conditions. At low
370 latitudes, it is worth noting that the ITCZ lies at the foot of the ascending branch of the meridional circulation, which is highly linked to the hemispheric asymmetry of the atmospheric energy budget (Frierson et al., 2013). We further quantify the shift of the ITCZ in Fig. 7(b) and Earth's energy budget in Fig. 7(c) and (d). The definition of the ITCZ location is the latitude of the maximal annual mean precipitation between 20°S and 20°S (Frierson and Hwang, 2012; Donohoe et al., 2013). On average, ensemble models show that the NH atmosphere receives 1.5 W·m^{-2} more net radiation than the SH (Fig. 7(d)),
375 which could induce an increased cross-equatorial southward energy flux of 0.22 PW (Fig. 7(e)). Thus, this imbalance in the

atmospheric energy budget causes a 1.1° northward shift in the zonal-mean ITCZ latitude. Consequently, this shift of the ITCZ reorganizes atmospheric circulation (Watt-Meyer and Frierson, 2019), leading to the northward movement of the meridional circulation in the SH (Fig. 7(a)). This meridional circulation shift could result in a weakened (strengthened) meridional circulation in the NH (SH) (Fig. 7(a)) and hence drive δMCD_{D_M} (Fig. 4(f)) and MMTD (Fig. 5(c)).
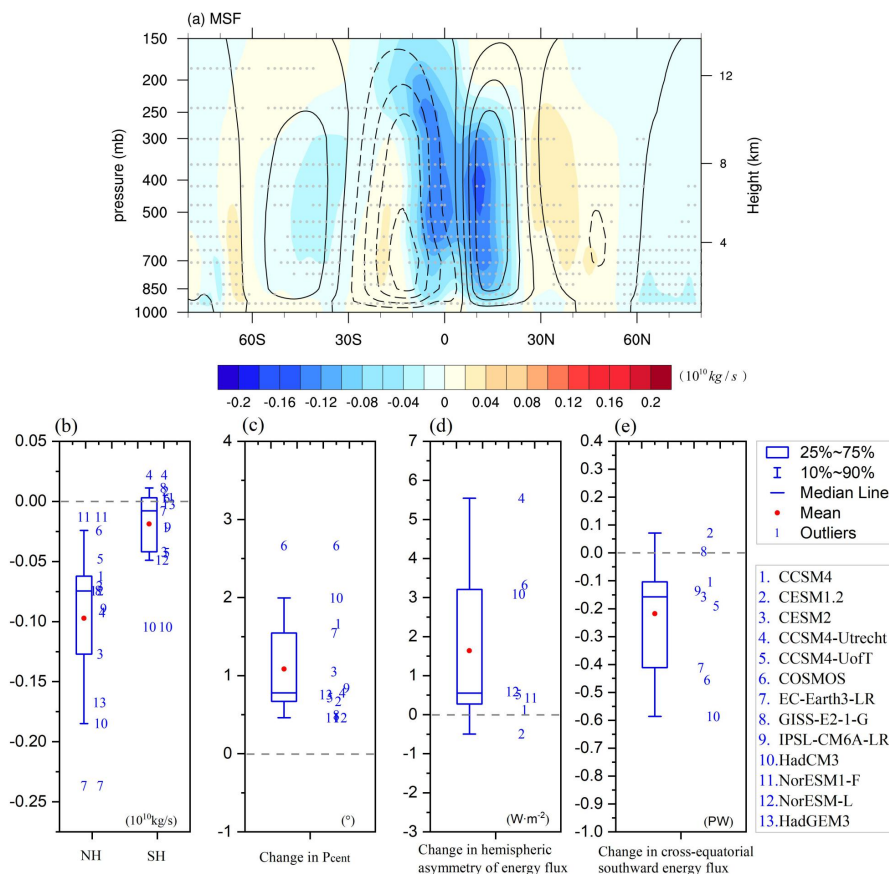
380

Figure 7: (a) Changes in annual mean MSF (shading; units: 10^{10} kg•s^{-1}) of meridional circulation for mid-Pliocene with respect to the PI simulation, overlaid by the climate mean MSF for the PI simulation (contours). The meridional wind $\vec{V}_M$ is decomposed from the 3P-DGAC method. Solid curves indicate positive values, and dashed curves indicate negative values. Stippling indicates regions where at least 10 of 13 simulations in the model group agree on the sign of the ensemble mean. (b) Changes in annual mean
385 **intensities (unit: 10^{10} kg/s) of meridional circulation in the NH and SH. (c) The latitudes of the center of annual mean precipitation between 20°S and 20°N (unit: °). (d) Hemispheric asymmetry (NH minus SH) of energy flux into the atmosphere (unit: W•m^{-2}). (e) Changes in the integrated atmospheric meridional heat transport across the equator (unit: PW).**
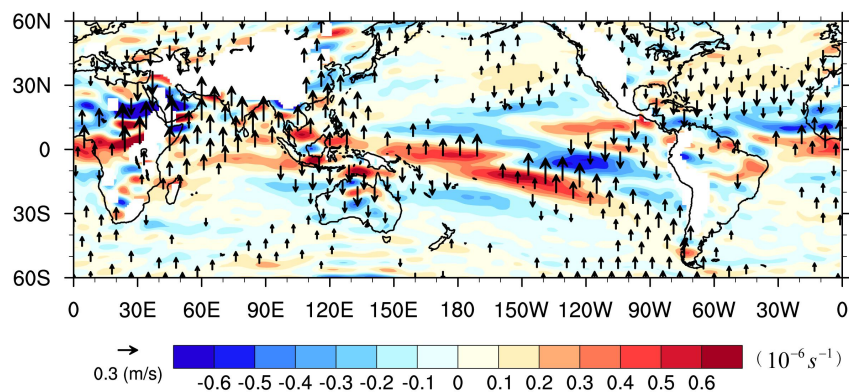
Figure 8: The changes in meridional wind $\vec{V}_M$ decomposed from the 3P-DGAC method at the 850 hPa level (vectors, units: m•s^{-1}),
overlaid by its divergent circulations (shading, units: 10^{-6} s^{-1}). Only vectors where at least 10 of 13 simulations in the model group
agree on the sign of the ensemble mean are shown here.

5.3 Response in zonal circulation

As mentioned above, δMCD_{D_Z} plays a key role in the changes in PmE over the northern Indian Ocean. As this term is

linked to Walker circulation anomalies, we further discuss Walker circulation changes in the mid-Pliocene warm climate.

There is a noticeable diversity in the simulated Pacific Walker circulation (PWC) intensity across the models, with

the mean PWC intensity strengthened by 1×10^{10} kg/m^2 compared with the PI simulation (Fig. 9(a)). In addition, previous

work has suggested that the PWC intensity is closely tied to the zonal SST and SLP gradient during the mid-Piacenzian

(Tierney et al., 2019). In this paper, the dSLP and dSST are defined as the difference in SLP and SST across the equatorial

Indo-Pacific (160°W-80°W, 5°S-5°N minus 80°E-160°E, 5°S-5°N). The PlioMIP2 models produce a large spread in

simulating the changes in dSST (Fig. 9(c)) and dSLP (Fig. 9(d)), which is consistent with the results in Fig. 9(a). Previous

studies have suggested that the east-west SST gradient was reduced in SST proxies (Tierney et al., 2019). This feature is

captured by the CESM2, GISS-E2-1-G and HadGEM3 models (Fig. 9(a)-(c)). However, other models, i.e., the CCSM4,

CCSM4-Utrecht, EC-Earth3-LR, and NorESM-L models, consistently simulated stronger PWC intensity (Fig. 9(a)-(c)). That

is, the results suggest that the model-simulated changes in the strength of PWC are probably highly model dependent, which

might be affected by the different parameterizations (Tierney et al., 2019).
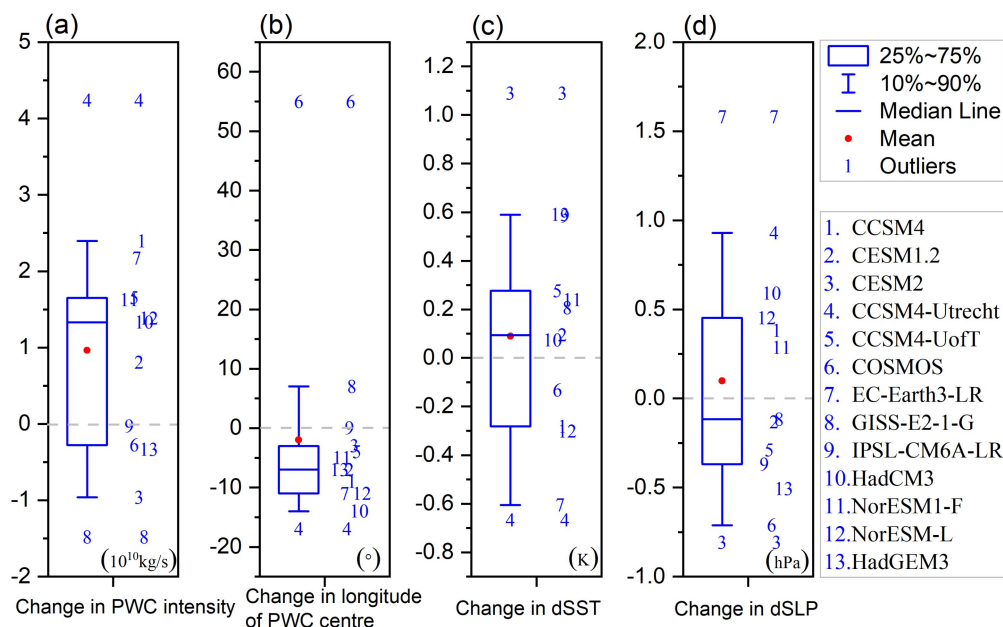
Figure 9: Changes in annual mean of the (a) intensities of Pacific Walker circulation (PWC; unit: 10^{10} kg/s), (b) longitude of the PWC cell center (units: °), (c) dSST (units: K), and (d) dSLP (units: hPa) for mid-Pliocene simulations compared with the PI simulation. Here, the PWC intensity is defined as the vertically integrated ZMS (Bayr et al., 2014; Schwendike et al., 2014) averaged in the equatorial Pacific (140°E-120°W), and the location of the PWC cell center is the longitude of the maximum ZMS. The dSLP and dSST are defined as the difference in SLP and SST across the equatorial Indo-Pacific (160°W-80°W, 5°S-5°N minus 80°E-160°E, 5°S-5°N).

However, the westward shift of PWC is a robust feature among these models except the COSMOS and GISS-E2-1-G models (Fig. 9(b)). To discuss the impact of the PWC shift on atmospheric circulation in the tropics, we further calculate the changes in the zonal mass stream function (ZMS) for the mid-Pliocene with respect to the PI simulation in Fig. 10. As suggested in Fig. 6(d), the ZMS in the PI simulation (contours in Fig. 10(a)) is characterized by ascending in the tropical western Pacific and Maritime Continent and descending in the western Indian Ocean and eastern Pacific, consistent with previous studies (Kamae et al., 2011; Bayr et al., 2014; Ma and Zhou, 2016; Han et al., 2020). Compared with the PI simulation, the most striking features in the mid-Pliocene simulation are weakened ascending over the Maritime Continent and tropical western Pacific and strengthened descending on the western Indian Ocean, indicating a westward movement of the PWC (Fig. 10(b)).
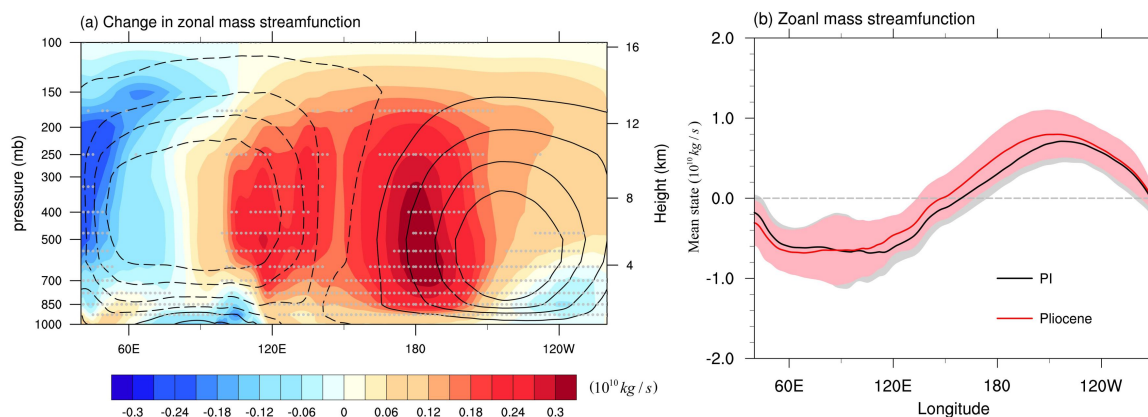
Figure 10: (a) Changes in ZMS (shading, unit: 10¹⁰ kg s⁻¹) averaged between 10°S/N for the mid-Pliocene with respect to the PI simulation, overlaid by the climate mean ZMS for the PI simulation (contours). The zonal wind $\vec{V}_Z$ is used to calculate ZMS, which is decomposed from the 3P-DGAC method. The contours represent the climate mean ZMS for the PI simulation. Solid curves indicate a positive value, and dashed curves show a negative value. Stippling indicates regions where at least 10 of 13 simulations in the model group agree on the sign of the ensemble mean. (b) is the vertical integrated ZMS in (a). The gray and pink shading indicates 1 standard deviation of individual models departure from the MMM mean of MSF for the PI and mid-Pliocene simulations, respectively.

The westward shift of the PWC can also be seen from the potential velocity (Fig. 11). This shows that the center of anomalous positive values is located in the northern Indian Ocean. In contrast, the center of a negative value exists in the equatorial eastern Pacific and western Atlantic in the low-level troposphere (Fig. 11(a)). Concurrent, generally opposite anomalies can be seen in the upper-level troposphere (Fig. 11(b)). Indeed, these features indicate an upward (downward) motion shift from the tropical western Pacific (eastern Pacific) to the west of the Indian Ocean (central Pacific), resulting from the westward shift of the PWC (Figs. 9(b) and 10). That is, when divergent/convergent circulations are combined with the climate mean specific humidity ($\overline{q} > 0$) in the lower troposphere, they can trigger a negative/positive contribution from the δMCD_{D_Z} term to changes in PmE (Fig. 4(g)).
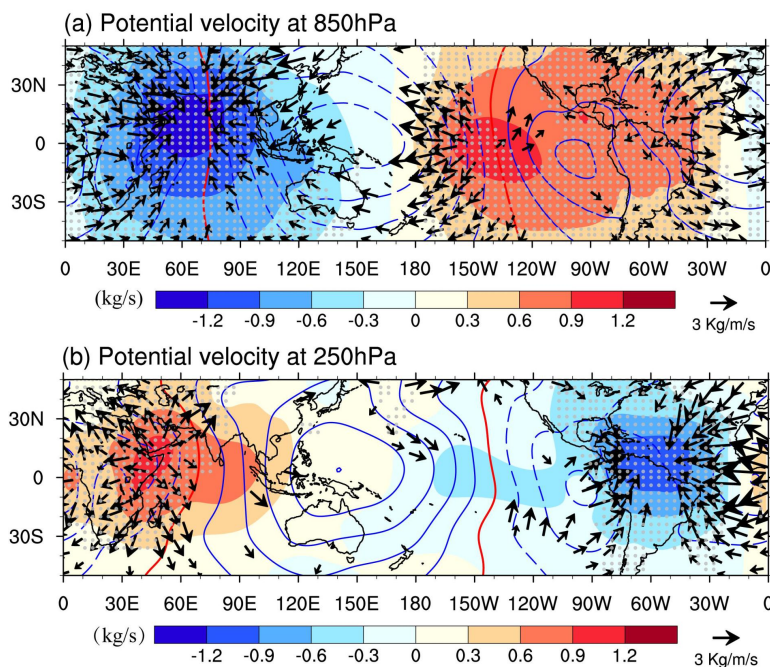
Figure 11: Changes in the potential function of zonal wind $\vec{V}_Z$ at (a) 850 hPa and (b) 250 hPa (shading, unit: kg/s), corresponding to the divergent mode of the wind field (vectors, unit: kg/m/s). $\vec{V}_Z$ is decomposed from the 3P-DGAC method. The contours represent the climate mean of the potential function for the PI simulation. Solid curves indicate positive values, and dashed curves indicate negative values. Red solid curves represent zero values. The vectors and stippled regions are where at least 10 of 13 simulations in the model group agree on the ensemble mean.

6 Conclusion and discussion

This paper evaluates the changes in the large-scale hydrological cycle during the mid-Pliocene with respect to the PI based on 13 PlioMIP2 simulations. A diagnostic analysis using the moisture budget equation and the Earth's energy budget provides insight into the mechanisms. The main conclusions are summarized as follows.

The PlioMIP2 models show large spatial differences in PmE. The MMM generally depicts a wet-regions-getting-wetter (i.e., ITCZ, Maritime Continent and monsoon regions) and-dry-regions-getting-drier (i.e., a sinking branch Hadley circulation) pattern during the mid-Pliocene warm climate. According to the moisture budget equation, a large part of the changes in PmE at low latitudes are due to the increased specific humidity. However, the thermodynamic component cannot fully explain the changes in PmE. The dynamic effects offset the thermodynamic effects to some extent and even determine a larger contribution to the changes in PmE in the southern tropical Pacific and northern Indian Ocean. We find increased hemispheric asymmetries of the atmospheric energy budget (larger atmospheric energy over NH than SH) during the mid-Pliocene compared with PI, which could induce the northward shift of the ITCZ and reorganize atmospheric circulation. These features can result in a weakening meridional circulation in the Northern Hemispheric monsoon regions and a

strengthening meridional circulation in the SH. In addition, the anomalous meridional circulation can dry the deep tropics
460 but moisten the northern part of the ITCZ. Furthermore, these anomalies dry the SPCZ region and wet its southern part,
which is associated with the southward shift of the SPCZ. We also find a robust westward shift in PWC, which appears to
moisten the northern Indian Ocean via anomalous convergence of zonal circulation.

Our analyses provide a relatively complete understanding of the changes in the large-scale hydrological cycle
within the PlioMIP2 ensemble. It is evident that in a warmer climate, the air could hold more moisture, and thus, the
465 thermodynamic effects amplify the intensity of PmE but do not alter its spatial pattern (Fig. 2(a); Held and Soden, 2006).
Note that the hemispheric asymmetries of atmospheric energy could induce regional meridional circulation anomalies and
thus alter the distribution of PmE anomalies during the mid-Pliocene via the δMCD_{D_M} term at low latitudes. The
PlioPMIP2 ensemble simulations suggest that hemispheric asymmetries of atmospheric energy are the key factor altering the
spatial pattern of PmE via changes in the local meridional circulation. However, we should note that a noticeable intermodel
470 spread exists in capturing the main features in the past warm climate, particularly for the changes in Walker circulation, such
as the large spread in the simulated changes in the intensity of PWC, dSST and dSLP in Fig. 9, consistent with previous
studies (Arthur et al., 2021). Further effort to understand the intermodel uncertainty needs to be investigated in future work.
In addition, previous studies indicate that the storm track (transient eddy component) may play a key role in changes in PmE
for mid- to high latitudes (Seager et al., 2010; Han et al., 2019a; Han et al., 2019b). Due to the lack of hourly model data, we
475 mainly discuss the relative contributions from moisture budget components to changes in PmE at low latitudes in this paper.
Much more work should be conducted to study the impact of storm tracks on changes in PmE during the mid-Pliocene using
hourly data in the future at mid-to-high latitudes.

Data availability. To access the PlioMIP2 database, please send a request to Alan M. Haywood (a.m.haywood@leeds.ac.uk). PlioMIP2 data from CESM2, EC-Earth3-LR, GISS-E2-1-G, IPSL-CM6A-LR and NorESM1-F can be obtained from the
480 Earth System Grid Federation (ESGF, 2020, https://esgf-node.llnl.gov/search/cmip6/). CCSM4 and CESM1.1 can be obtained from https://www.cesm.ucar.edu/models/. The reconstructed SST is from the alkenone-derived $U_{37}^{K'}$ index and foraminifera calcite Mg/Ca and can be accessed from https://pliovar.github.io/km5c.html.

Author contributions. Qiong Zhang and Zixuan Han designed the work, Zixuan Han wrote the manuscript under supervision from Qiong Zhang. Zixuan Han did the analyses and programming with the help of Jianbo Cheng and Qin Wen. All the
485 other co-authors provided the PlioMIP2 model data and commented on the manuscript.

Competing interests. The authors declare that they have no conflict of interest.

Special issue statement. This article is part of the special issue "PlioMIP Phase 2: experimental design, implementation and scientifific results". It is not associated with a conference.

Acknowledgements. This research has been supported by "the Fundamental Research Funds for the Central Universities":
490 B210201009 and the Swedish Research Council (Vetenskapsrådet, grant no. 2013-06476 and 2017-04232). CJ acknowledges financial support from the National Natural Science Foundation of China (Grant No. 42005012) and the Natural Science Foundation of Jiangsu Province (Grant No.BK20201058). The model simulations with EC-Earth3 and data analysis were performed using ECMWF's computing and archive facilities and the Swedish National Infrastructure for Computing (SNIC) at the National Supercomputer Centre (NSC) partially funded by the Swedish Research Council through
495 grant agreement no. 2018-05973. CJRW acknowledges the financial support of the UK Natural Environment Research Council funded SWEET project (Super-Warm Early Eocene Temperatures), research grant NE/P01903X/1. NJB acknowledges supported from the National Science Foundation (NSF; AGS-1844380 and OCN-2002448), as well as the Alfred P. Sloan Foundation as a Research Fellow. RF acknowledges the sponsorship by U.S. National Science Foundation grants 1903650 and 1814029. The contributions of BLO-B, ECB, and NR are based upon work supported by the National
500 Center for Atmospheric Research, which is a major facility sponsored by the NSF under Cooperative Agreement No. 1852977. The CESM project is supported primarily by the National Science Foundation (NSF). Computing and data storage resources for the CESM and CCSM4 simulaitons, including the Cheyenne supercomputer (doi:10.5065/D6RX99HX), were provided by the Computational and Information Systems Laboratory (CISL) at NCAR. XL acknowledges financial support from the National Natural Science Foundation of China (NSFC, grant no. 42005042) and China Scholarship Council
505 (201804910023). The NorESM simulations benefitted from resources provided by UNINETT Sigma2–the National Infrastructure for High Performance Computing and Data Storage in Norway. The work by ASvdH and MLJB was carried out under the program of the Netherlands Earth System Science Centre (NESSC), financially supported by the Ministry of Education, Culture and Science (OCW grant no. 024.002.001). Simulations with CCSM4-Utrecht were performed at the SURFsara Dutch national computing facilities and were sponsored by NWO-EW (Netherlands Organisation for Scientific
510 Research, Exact Sciences) (project no. 17189). The PRISM4 reconstruction and boundary conditions used in PlioMIP2 were funded by the U.S. Geological Survey Climate and Land Use Change Research and Development Program. Any use of trade, firm, or product names is for descriptive purposes only and does not imply endorsement by the U.S. Government.

515

References

Allen, M. R. and Ingram, W. J.: Constraints on future changes in climate and the hydrologic cycle, Nature, 419, 224–232, https://doi.org/10.1038/nature01092, 2002.

Asokan, S. M. and Destouni, G.: Irrigation effects on hydro-climatic change: basin-wise water balance-constrained
520   quantification and cross-regional comparison, Surv. Geophy., 35, 879–895, https://doi.org/10.1007/s10712-013-9223-5, 2014.

Arthur Merlijn Oldeman, Michiel L. J. Baatsen, Anna S. von der Heydt, Henk A. Dijkstra, Julia C. Tindall, Ayako Abe-Ouchi, Alice R. Booth, Esther C. Brady, Wing-Le Chan, Deepak Chandan, Mark A. Chandler, Camille Contoux, Ran Feng, Chuncheng Guo, Alan M. Haywood, Stephen J. Hunter, Youichi Kamae, Qiang Li, Xiangyu Li, Gerrit
525   Lohmann, Daniel J. Lunt, Kerim H. Nisancioglu, Bette L. Otto-Bliesner, W. Richard Peltier, Gabriel M. Pontes, Gilles Ramstein, Linda E. Sohl, Christian Stepanek, Ning Tan, Qiong Zhang, Zhongshi Zhang, Ilana Wainer, and Charles J. R. Williams.: Reduced El Niño variability in the mid-Pliocene according to the PlioMIP2 ensemble. In prep, 2021.

Baatsen, M., Von der Heydt, A., Kliphuis, M., Oldeman, A., and Weiffenbach, J.: Warm mid-Pliocene conditions using the
530   CESM 1.0.4: the utrecht contribution to the PlioMIP2 ensemble, in prep. 2021.

Bayr, T., Dommenget, D., Martin, T., and Power, S. B.: The eastward shift of the Walker circulation in response to global warming and its relationship to ENSO variability, Clim. Dynam., 43, 2747–2763, https://doi.org/10.1007/s00382-014-2091-y, 2014.

Bengtsson, L.: Foreword: International Space Science Institute (ISSI) workshop on the earth's hydrological cycle, in: The
535   Earth's Hydrological Cycle, edited by: Bengtsson, L., Bonnet, R. M., Calisto, M., Destouni, G., Gurney, R., Johannessen, J., Kerr, Y., Lahoz, W. A., and Rast, M., Springer, Dordrecht, Netherlands, 485–488, https://doi.org/10.1007/978-94-017-8789-5_1, 2014.

Burke, K. D., Williams, J. W., Chandler, M. A., Haywood, A. M., Lunt, D. J., and Otto-Bliesner, B. L.: Pliocene and Eocene provide best analogs for near-future climates, Proc. Natl. Acad. Sci. U. S. A., 115, 13288,
540   https://doi.org/10.1073/pnas.1809600115, 2018.

Burls, N. J. and Fedorov, A. V.: Wetter subtropics in a warmer world: contrasting past and future hydrological cycles, Proc. Natl. Acad. Sci. U. S. A., 114, 12888, https://doi.org/10.1073/pnas.1703421114, 2017.

Chandan, D. and Peltier, W. R.: Regional and global climate for the mid-Pliocene using the University of Toronto version of CCSM4 and PlioMIP2 boundary conditions, Clim. Past, 13, 919–942, https://doi.org/10.5194/cp-13-919-2017,
545   2017.

Cheng, J., Hu, S., Gao, C., Hou, X., Xu, Z., and Feng, G.: On the discrepancies in the changes in the annual mean Hadley circulation among different regions and between CMIP5 models and reanalyses, Theor. Appl. Climatol., 141, 1475–1491, https://doi.org/10.1007/s00704-020-03292-3, 2020.

Chou, C., Neelin, J. D., Chen, C. A., and Tu, J. Y.: Evaluating the "Rich-Get-Richer" mechanism in tropical precipitation
550 change under global warming, J. Climate, 22, 1982–2005, https://doi.org/10.1175/2008JCLI2471.1, 2009.

Corvec, S. and Fletcher, C.: Changes to the tropical circulation in the mid-Pliocene and their implications for future climate, Clim. Past, 13, 135–147, https://doi.org/10.5194/cp-13-135-2017, 2017.

De Nooijer, W., Zhang, Q., Li, Q., Zhang, Q., Li, X., Zhang, Z., Guo, C., Nisancioglu, K. H., Haywood, A. M., Tindall, J. C., Hunter, S. J., Dowsett, H. J., Stepanek, C., Lohmann, G., Otto-Bliesner, B. L., Feng, R., Sohl, L. E., Chandler, M.
555 A., Tan, N., Contoux, C., Ramstein, G., Baatsen, M. L. J., Von der Heydt, A. S., Chandan, D., Peltier, W. R., Abe-Ouchi, A., Chan, W. L., Kamae, Y., and Brierley, C. M.: Evaluation of Arctic warming in mid-Pliocene climate simulations, Clim. Past, 16, 2325–2341, https://doi.org/10.5194/cp-16-2325-2020, 2020.

Delaney, M.L., Bé, A.W. and Boyle, E.A.: Li, Sr, Mg, and Na in foraminiferal calcite shells from laboratory culture, sediment traps, and sediment cores. Geochimica et Cosmochimica Acta, 49, 1327-1341,
560 https://doi.org/10.1016/0016-7037(85)90284-4, 1985.

Donohoe, A., Marshall, J., Ferreira, D., and McGee, D.: The relationship between ITCZ location and cross-equatorial atmospheric heat transport: from the seasonal cycle to the last glacial maximum, J. Clim., 26, 3597–3618, https://doi.org/10.1175/JCLI-D-12-00467.1, 2013.

Dowsett, H., Dolan, A., Rowley, D., Moucha, R., Forte, A. M., Mitrovica, J. X., Pound, M., Salzmann, U., Robinson, M.,
565 Chandler, M., Foley, K., and Haywood, A.: The PRISM4 (mid-Piacenzian) paleoenvironmental reconstruction, Clim. Past, 12, 1519–1538, https://doi.org/10.5194/cp-12-1519-2016, 2016.

Dowsett, H. J., Robinson, M. M., Haywood, A. M., Hill, D. J., Dolan, A. M., Stoll, D. K., Chan, W. L., Abe-Ouchi, A., Chandler, M. A., Rosenbloom, N. A., Otto-Bliesner, B. L., Bragg, F. J., Lunt, D. J., Foley, K. M., and Riesselman, C. R.: Assessing confidence in Pliocene sea surface temperatures to evaluate predictive models, Nat. Clim. Change,
570 2, 365–371, https://doi.org/10.1038/nclimate1455, 2012.

Eltahir, E. A. B. and Bras, R. L.: Precipitation recycling, Rev. Geophys., 34, 367–378, https://doi.org/10.1029/96RG01927, 1996.

Feng, R., Otto-Bliesner, B. L., Brady, E. C., and Rosenbloom, N.: Increased climate response and earth system sensitivity from CCSM4 to CESM2 in mid-Pliocene simulations, J. Adv. Model. Earth Sy., 12, e2019MS002033,
575 https://doi.org/10.1029/2019MS002033, 2020.

Feng, R., Otto-Bliesner, B. L., Fletcher, T. L., Tabor, C. R., Ballantyne, A. P., and Brady, E. C.: Amplified late Pliocene terrestrial warmth in northern high latitudes from greater radiative forcing and closed Arctic Ocean gateways, Earth Planet. Sc. Lett., 466, 129–138, https://doi.org/10.1016/j.epsl.2017.03.006, 2017.

Frierson, D. M. W. and Hwang, Y. T.: Extratropical influence on ITCZ shifts in slab ocean simulations of global warming, J.
580   Clim., 25, 720–733, https://doi.org/10.1175/JCLI-D-11-00116.1, 2012.

Frierson, D. M. W., Hwang, Y. T., Fučkar, N. S., Seager, R., Kang, S. M., Donohoe, A., Maroon, E. A., Liu, X., and Battisti,
D. S.: Contribution of ocean overturning circulation to tropical rainfall peak in the Northern Hemisphere, Nat.
Geosci., 6, 940–944, https://doi.org/10.1038/ngeo1987, 2013.

Han, Z., Su, T., Huang, B., Feng, T., Qu, S., and Feng, G.: Changes in global monsoon precipitation and the related dynamic
585   and thermodynamic mechanisms in recent decades, Int. J. Climatol., 39, 1490–1503,
https://doi.org/10.1002/joc.5896, 2019a.

Han, Z., Su, T., Zhang, Q., Wen, Q., and Feng, G.: Thermodynamic and dynamic effects of increased moisture sources over
the Tropical Indian Ocean in recent decades, Clim. Dynam., 53, 7081–7096, https://doi.org/10.1007/s00382-019-
04977-w, 2019b.

590   Han, Z., Zhang, Q., Wen, Q., Lu, Z., Feng, G., Su, T., Li, Q., and Zhang, Q.: The changes in ENSO-induced tropical Pacific
precipitation variability in the past warm and cold climates from the EC-Earth simulations, Clim. Dynam., 55, 503–
519, https://doi.org/10.1007/s00382-020-05280-9, 2020.

Hastenrath, S.: Climate Dynamics of the Tropics, Kluwer Academic Publishers, Dordrecht, Netherlands, 1991.

Haywood, A. M., Dowsett, H. J., Dolan, A. M., Rowley, D., Abe-Ouchi, A., Otto-Bliesner, B., Chandler, M. A., Hunter, S. J.,
595   Lunt, D. J., Pound, M., and Salzmann, U.: The Pliocene Model Intercomparison Project (PlioMIP) phase 2:
scientific objectives and experimental design, Clim. Past, 12, 663–675, https://doi.org/10.5194/cp-12-663-2016,
2016.

Haywood, A. M., Hill, D. J., Dolan, A. M., Otto-Bliesner, B. L., Bragg, F., Chan, W. L., Chandler, M. A., Contoux, C.,
Dowsett, H. J., Jost, A., Kamae, Y., Lohmann, G., Lunt, D. J., Abe-Ouchi, A., Pickering, S. J., Ramstein, G.,
600   Rosenbloom, N. A., Salzmann, U., Sohl, L., Stepanek, C., Ueda, H., Yan, Q., and Zhang, Z.: Large-scale features of
Pliocene climate: results from the Pliocene model intercomparison project, Clim. Past, 9, 191–209,
https://doi.org/10.5194/cp-9-191-2013, 2013.

Haywood, A. M., Tindall, J. C., Dowsett, H. J., Dolan, A. M., Foley, K. M., Hunter, S. J., Hill, D. J., Chan, W. L., Abe-
Ouchi, A., Stepanek, C., Lohmann, G., Chandan, D., Peltier, W. R., Tan, N., Contoux, C., Ramstein, G., Li, X.,
605   Zhang, Z., Guo, C., Nisancioglu, K. H., Zhang, Q., Li, Q., Kamae, Y., Chandler, M. A., Sohl, L. E., Otto-Bliesner,
B. L., Feng, R., Brady, E. C., Von der Heydt, A. S., Baatsen, M. L. J., and Lunt, D. J.: The Pliocene model
intercomparison project phase 2: large-scale climate features and climate sensitivity, Clim. Past, 16, 2095–2123,
https://doi.org/10.5194/cp-16-2095-2020, 2020.

Held, I. M. and Soden, B. J.: Robust responses of the hydrological cycle to global warming, J. Clim., 19, 5686–5699,
610   https://doi.org/10.1175/JCLI3990.1, 2006.

Howell, F. W., Haywood, A. M., Dowsett, H. J., and Pickering, S. J.: Sensitivity of Pliocene Arctic climate to orbital forcing, atmospheric CO_2 and sea ice albedo parameterisation, Earth Planet. Sc. Lett., 441, 133–142, https://doi.org/10.1016/j.epsl.2016.02.036, 2016.

Hu, S., Cheng, J., and Chou, J.: Novel three-pattern decomposition of global atmospheric circulation: generalization of
615   traditional two-dimensional decomposition, Clim. Dynam., 49, 3573–3586, https://doi.org/10.1007/s00382-017-3530-3, 2017.

Hu, S., Cheng, J., Xu, M., and Chou, J.: Three-pattern decomposition of global atmospheric circulation: part II—dynamical equations of horizontal, meridional and zonal circulations, Clim. Dynam., 50, 2673–2686, https://doi.org/10.1007/s00382-017-3763-1, 2018c.

620 Hu, S., Chou, J., and Cheng, J.: Three-pattern decomposition of global atmospheric circulation: part I—decomposition model and theorems, Clim. Dynam., 50, 2355–2368, https://doi.org/10.1007/s00382-015-2818-4, 2018b.

Hu, Y., Huang, H., and Zhou, C.: Widening and weakening of the Hadley circulation under global warming, Sci. Bull., 63, 640–644, https://doi.org/10.1016/j.scib.2018.04.020, 2018a.

Hunter, S. J., Haywood, A. M., Dolan, A. M., and Tindall, J. C.: The HadCM3 contribution to PlioMIP phase 2, Clim. Past,
625   15, 1691–1713, https://doi.org/10.5194/cp-15-1691-2019, 2019.

Kamae, Y., Ueda, H., and Kitoh, A.: Hadley and Walker circulations in the mid-Pliocene warm period simulated by an atmospheric general circulation model, J. Meteorol. Soc. Jpn. Ser. II, 89, 475–493, https://doi.org/10.2151/jmsj.2011-505, 2011.

Li, G., Harrison, S. P., Bartlein, P. J., Izumi, K., and Colin Prentice, I.: Precipitation scaling with temperature in warm and
630   cold climates: an analysis of CMIP5 simulations, Geophys. Res. Lett., 40, 4018–4024, https://doi.org/10.1002/grl.50730, 2013.

Li, X., Jiang, D., Zhang, Z., Zhang, R., Tian, Z., Yan, Q.: Mid-Pliocene westerlies from PlioMIP simulations. Advances in Atmospheric Sciences, 32, 909–923, doi:10.1007/s00376-014-4171-7, 2015.

Xiangyu Li, Dabang Jiang, Zhiping Tian, Yibo Yang.: Mid-Pliocene global land monsoon from PlioMIP1 simulations.
635   Palaeogeography, Palaeoclimatology, Palaeoecology, 512, 56–70, 2018.

Li, X., Guo, C., Zhang, Z., Otterå, O. H., and Zhang, R.: PlioMIP2 simulations with NorESM-L and NorESM1-F, Clim. Past, 16, 183–197, https://doi.org/10.5194/cp-16-183-2020, 2020.

Long, S. M., Xie, S. P., Zheng, X. T., and Liu, Q.: Fast and slow responses to global warming: sea surface temperature and precipitation patterns, J. Clim., 27, 285–299, https://doi.org/10.1175/JCLI-D-13-00297.1, 2014.

640 Long, S.M., Xie, S.P. and Liu, W.: Uncertainty in tropical rainfall projections: Atmospheric circulation effect and the ocean coupling, J. Clim., 29, 2671-2687, https://doi.org/10.1175/JCLI-D-15-0601.1, 2016.

Lu, J., Yang, H., Griffiths, M. L., Burls, N. J., Xiao, G., Yang, J., Wang, J. K., Johnson, K. R., and Xie, S.: Asian monsoon evolution linked to Pacific temperature gradients since the Late Miocene, Earth Planet. Sc. Lett., 563, 116882, https://doi.org/10.1016/j.epsl.2021.116882, 2021.

645   Lurton, T., Balkanski, Y., Bastrikov, V., Bekki, S., Bopp, L., Braconnot, P., Brockmann, P., Cadule, P., Contoux, C., Cozic, A., Cugnet, D., Dufresne, J. L., Éthé, C., Foujols, M. A., Ghattas, J., Hauglustaine, D., Hu, R. M., Kageyama, M., Khodri, M., Lebas, N., Levavasseur, G., Marchand, M., Ottlé, C., Peylin, P., Sima, A., Szopa, S., Thiéblemont, R., Vuichard, N., and Boucher, O.: Implementation of the CMIP6 forcing data in the IPSL-CM6A-LR model, J. Adv. Model. Earth Sy., 12, e2019MS001940, https://doi.org/10.1029/2019MS001940, 2020.

650   Ma, S. and Zhou, T.: Robust strengthening and westward shift of the tropical Pacific Walker circulation during 1979–2012: a comparison of 7 sets of reanalysis data and 26 CMIP5 models, J. Clim., 29, 3097–3118, https://doi.org/10.1175/JCLI-D-15-0398.1, 2016.

McClymont, E. L., Ford, H. L., Ho, S. L., Tindall, J. C., Haywood, A. M., Alonso-Garcia, M., Bailey, I., Berke, M. A., Littler, K., Patterson, M. O., Petrick, B., Peterse, F., Ravelo, A. C., Risebrobakken, B., De Schepper, S., Swann, G.
655   E. A., Thirumalai, K., Tierney, J. E., Van der Weijst, C., White, S., Abe-Ouchi, A., Baatsen, M. L. J., Brady, E. C., Chan, W. L., Chandan, D., Feng, R., Guo, C., Von der Heydt, A. S., Hunter, S., Li, X., Lohmann, G., Nisancioglu, K. H., Otto-Bliesner, B. L., Peltier, W. R., Stepanek, C., and Zhang, Z.: Lessons from a high-CO_2 world: an ocean view from ∼ 3 million years ago, Clim. Past, 16, 1599–1615, https://doi.org/10.5194/cp-16-1599-2020, 2020.

Oort, A. H. and Yienger, J. J.: Observed interannual variability in the Hadley circulation and its connection to ENSO, J.
660   Clim., 9, 2751–2767, https://doi.org/10.1175/1520-0442(1996)009<2751:OIVITH>2.0.CO;2, 1996.

Otto-Bliesner, B. L., Brady, E. C., Fasullo, J., Jahn, A., Landrum, L., Stevenson, S., Rosenbloom, N., Mai, A., and Strand, G.: Climate variability and change since 850 CE: an ensemble approach with the community earth system model, B. Am. Meteorol. Soc., 97, 735–754, https://doi.org/10.1175/BAMS-D-14-00233.1, 2016.

Peixoto, J. and Oort, A.: The Physics of Climate, AIP Press, New York, NY, 1992.

665   Pontes, G. M., Wainer, I., Taschetto, A. S., Sen Gupta, A., Abe-Ouchi, A., Brady, E. C., Chan, W. L., Chandan, D., Contoux, C., Feng, R., Hunter, S. J., Kame, Y., Lohmann, G., Otto-Bliesner, B. L., Peltier, W. R., Stepanek, C., Tindall, J., Tan, N., Zhang, Q., and Zhang, Z.: Drier tropical and subtropical Southern Hemisphere in the mid-Pliocene warm period, Sci. Rep., 10, 13458, https://doi.org/10.1038/s41598-020-68884-5, 2020.

Prahl, F.G. and Wakeham, S.G.: Calibration of unsaturation patterns in long-chain ketone compositions for
670   palaeotemperature assessment. Nature, 330, 367–369, https://doi.org/10.1038/330367a0, 1987.

Prescott, C. L., Haywood, A. M., Dolan, A. M., Hunter, S. J., and Tindall, J. C.: Indian monsoon variability in response to orbital forcing during the late Pliocene, Global Planet. Change, 173, 33–46, https://doi.org/10.1016/j.gloplacha.2018.12.002, 2019.

Previdi, M. and Liepert, B. G.: Annular modes and Hadley cell expansion under global warming, Geophys. Res. Lett., 34,
675   L22701, https://doi.org/10.1029/2007GL031243, 2007.

Root, T. L., Price, J. T., Hall, K. R., Schneider, S. H., Rosenzweig, C., and Pounds, J. A.: Fingerprints of global warming on wild animals and plants, Nature, 421, 57–60, https://doi.org/10.1038/nature01333, 2003.

Salzmann, U., Dolan, A. M., Haywood, A. M., Chan, W. L., Voss, J., Hill, D. J., Abe-Ouchi, A., Otto-Bliesner, B., Bragg, F. J., Chandler, M. A., Contoux, C., Dowsett, H. J., Jost, A., Kamae, Y., Lohmann, G., Lunt, D. J., Pickering, S. J., Pound, M. J., Ramstein, G., Rosenbloom, N. A., Sohl, L., Stepanek, C., Ueda, H., and Zhang, Z.: Challenges in quantifying Pliocene terrestrial warming revealed by data–model discord, Nat. Clim. Change, 3, 969–974, https://doi.org/10.1038/nclimate2008, 2013.

Salzmann, U., Haywood, A. M., Lunt, D. J., Valdes, P. J., and Hill, D. J.: A new global biome reconstruction and data-model comparison for the middle Pliocene, Global Ecol. Biogeogr., 17, 432–447, https://doi.org/10.1111/j.1466-8238.2008.00381.x, 2008.

Samakinwa, E.: Modelling Mid-Pliocene Climate with COSMOS Based on PlioMIP2 Boundary Conditions, Master thesis, Institute of Environmental Physics (IUP), University of Bremen, Bremen, 2018.

Samakinwa, E., Stepanek, C., and Lohmann, G.: Sensitivity of mid-Pliocene climate to changes in orbital forcing and PlioMIP's boundary conditions, Clim. Past, 16, 1643–1665, https://doi.org/10.5194/cp-16-1643-2020, 2020.

Sanyal, P., Bhattacharya, S. K., Kumar, R., Ghosh, S. K., and Sangode, S. J.: Mio–Pliocene monsoonal record from Himalayan foreland basin (Indian Siwalik) and its relation to vegetational change, Palaeogeogr. Palaeocl., 205, 23–41, https://doi.org/10.1016/j.palaeo.2003.11.013, 2004.

Schwendike, J., Govekar, P., Reeder, M. J., Wardle, R., Berry, G. J., and Jakob, C.: Local partitioning of the overturning circulation in the tropics and the connection to the Hadley and Walker circulations, J. Geophys. Res. Atmos., 119, 1322–1339, https://doi.org/10.1002/2013JD020742, 2014.

Scroxton, N., Bonham, S. G., Rickaby, R. E. M., Lawrence, S. H. F., Hermoso, M., and Haywood, A. M.: Persistent El Niño–Southern Oscillation variation during the Pliocene Epoch, Paleoceanography, 26, PA2215, https://doi.org/10.1029/2010PA002097, 2011.

Seager, R., Naik, N., and Vecchi, G. A.: Thermodynamic and dynamic mechanisms for large-scale changes in the hydrological cycle in response to global warming, J. Clim., 23, 4651–4668, https://doi.org/10.1175/2010JCLI3655.1, 2010.

Sharmila, S. and Walsh, K. J. E.: Recent poleward shift of tropical cyclone formation linked to Hadley cell expansion, Nat. Clim. Change, 8, 730–736, https://doi.org/10.1038/s41558-018-0227-5, 2018.

Smith, D. M., Screen, J. A., Deser, C., Cohen, J., Fyfe, J. C., García-Serrano, J., Jung, T., Kattsov, V., Matei, D., Msadek, R., Peings, Y., Sigmond, M., Ukita, J., Yoon, J. H., and Zhang, X.: The Polar Amplification Model Intercomparison Project (PAMIP) contribution to CMIP6: investigating the causes and consequences of polar amplification, Geosci. Model Dev., 12, 1139–1164, https://doi.org/10.5194/gmd-12-1139-2019, 2019.

Stepanek, C., Samakinwa, E., Knorr, G., and Lohmann, G.: Contribution of the coupled atmosphere–ocean–sea ice–vegetation model COSMOS to the PlioMIP2, Clim. Past, 16, 2275–2323, https://doi.org/10.5194/cp-16-2275-2020, 2020.

Stephens, G. L. and Ellis, T. D.: Controls of global-mean precipitation increases in global warming GCM experiments, J. Clim., 21, 6141–6155, https://doi.org/10.1175/2008JCLI2144.1, 2008.

Stuecker, M. F., Bitz, C. M., Armour, K. C., Proistosescu, C., Kang, S. M., Xie, S. P., Kim, D., McGregor, S., Zhang, W., Zhao, S., Cai, W., Dong, Y., and Jin, F. F.: Polar amplification dominated by local forcing and feedbacks, Nat. Clim. Change, 8, 1076–1081, https://doi.org/10.1038/s41558-018-0339-y, 2018.

Sun, Y., Ramstein, G., Contoux, C., and Zhou, T.: A comparative study of large-scale atmospheric circulation in the context of a future scenario (RCP4.5) and past warmth (mid-Pliocene), Clim. Past, 9, 1613–1627, https://doi.org/10.5194/cp-9-1613-2013, 2013b.

Sun, Y., Zhou, T., and Zhang, L.: Observational analysis and numerical simulation of the interannual variability of the boreal winter Hadley circulation over the recent 30 years, Sci. China Earth Sci., 56, 647–661, https://doi.org/10.1007/s11430-012-4497-x, 2013a.

Tierney, J. E., Haywood, A. M., Feng, R., Bhattacharya, T., and Otto-Bliesner, B. L.: Pliocene warmth consistent with greenhouse gas forcing, Geophys. Res. Lett., 46, 9136–9144, https://doi.org/10.1029/2019GL083802, 2019.

Trauth, M. H., Maslin, M. A., Deino, A. L., Strecker, M. R., Bergner, A. G. N., and Dühnforth, M.: High- and low-latitude forcing of Plio-Pleistocene East African climate and human evolution, J. Hum. Evol., 53, 475–486, https://doi.org/10.1016/j.jhevol.2006.12.009, 2007.

Vallis, G. K., Zurita-Gotor, P., Cairns, C., and Kidston, J.: Response of the large-scale structure of the atmosphere to global warming, Q. J. Roy. Meteor. Soc., 141, 1479–1501, https://doi.org/10.1002/qj.2456, 2015.

Wan, S., Tian, J., Steinke, S., Li, A., and Li, T.: Evolution and variability of the East Asian summer monsoon during the Pliocene: evidence from clay mineral records of the South China sea, Palaeogeogr. Palaeocl., 293, 237–247, https://doi.org/10.1016/j.palaeo.2010.05.025, 2010.

Wang, B., Liu, J., Kim, H. J., Webster, P. J., and Yim, S. Y.: Recent change of the global monsoon precipitation (1979–2008), Clim. Dynam., 39, 1123–1135, https://doi.org/10.1007/s00382-011-1266-z, 2012.

Wara, M. W., Ravelo, A. C., and Delaney, M. L.: Permanent El Niño-like conditions during the Pliocene warm period, Science, 309, 758–761, https://doi.org/10.1126/science.1112596, 2005.

Watt-Meyer, O. and Frierson, D. M. W.: ITCZ width controls on Hadley cell extent and Eddy-Driven jet position and their response to warming, J. Clim., 32, 1151–1166, https://doi.org/10.1175/JCLI-D-18-0434.1, 2019.

Wentz, F. J., Ricciardulli, L., Hilburn, K., and Mears, C.: How much more rain will global warming bring? Science, 317, 233–235, https://doi.org/10.1126/science.1140746, 2007.

Williams, C. J. R., Sellar, A. A., Ren, X., Haywood, A. M., Hopcroft, P., Hunter, S. J., Roberts, W. H. G., Smith, R. S., Stone, E. J., Tindall, J. C., and Lunt, D. J.: Simulation of the mid-Pliocene warm period using HadGEM3: experimental design and results from model-model and model-data comparison, Clim. Past Discuss., 2021, 1–45, https://doi.org/10.5194/cp-2021-40, 2021.

Xie, S. P., Deser, C., Vecchi, G. A., Ma, J., Teng, H., and Wittenberg, A. T.: Global warming pattern formation: sea surface temperature and rainfall, J. Clim., 23, 966–986, https://doi.org/10.1175/2009JCLI3329.1, 2010.

Xie, S., Sun, B., Wu, J., Lin, Z., Yan, D., and Xiao, L.: Palaeodimatic estimates for the late Pliocene based on leaf physiognomy from Western Yunnan, China, Turk. J. Earth Sci., 21, 251–261, https://doi.org/10.3906/yer-1003-23, 2012.

Yan, Q., Zhang, Z. S., and Gao, Y. Q.: An East Asian Monsoon in the Mid-Pliocene, Atmos. Ocean. Sci. Lett., 5, 449–454, https://doi.org/10.1080/16742834.2012.11447034, 2012.

Zhang, Q., Berntell, E., Axelsson, J., Chen, J., Han, Z., De Nooijer, W., Lu, Z., Li, Q., Zhang, Q., Wyser, K., and Yang, S.: Simulating the mid-Holocene, last interglacial and mid-Pliocene climate with EC-Earth3-LR, Geosci. Model Dev., 14, 1147–1169, https://doi.org/10.5194/gmd-14-1147-2021, 2021a.

Zhang, R., Yan, Q., Zhang, Z. S., Jiang, D., Otto-Bliesner, B. L., Haywood, A. M., Hill, D. J., Dolan, A. M., Stepanek, C., Lohmann, G., Contoux, C., Bragg, F., Chan, W. L., Chandler, M. A., Jost, A., Kamae, Y., Abe-Ouchi, A., Ramstein, G., Rosenbloom, N. A., Sohl, L., and Ueda, H.: Mid-Pliocene East Asian monsoon climate simulated in the PlioMIP, Clim. Past, 9, 2085–2099, https://doi.org/10.5194/cp-9-2085-2013, 2013.

Zhang, R., Jiang, D., Zhang, Z., Yan, Q. and Li, X.: Modeling the late Pliocene global monsoon response to individual boundary conditions. Clim Dyn, 53, 4871-4886, https://doi.org/10.1007/s00382-019-04834-w,2019.

Zhang, Z., Li, X., Guo, C., Otterå, O. H., Nisancioglu, K. H., Tan, N., Contoux, C., Ramstein, G., Feng, R., Otto-Bliesner, B. L., Brady, E., Chandan, D., Peltier, W. R., Baatsen, M. L. J., Von der Heydt, A. S., Weiffenbach, J. E., Stepanek, C., Lohmann, G., Zhang, Q., Li, Q., Chandler, M. A., Sohl, L. E., Haywood, A. M., Hunter, S. J., Tindall, J. C., Williams, C., Lunt, D. J., Chan, W. L., and Abe-Ouchi, A.: Mid-Pliocene Atlantic meridional overturning circulation simulated in PlioMIP2, Clim. Past, 17, 529–543, https://doi.org/10.5194/cp-17-529-2021, 2021b.

Zheng, J., Zhang, Q., Li, Q., Zhang, Q., and Cai, M.: Contribution of sea ice albedo and insulation effects to Arctic amplification in the EC-Earth Pliocene simulation, Clim. Past, 15, 291–305, https://doi.org/10.5194/cp-15-291-2019, 2019.